

## **Paleomagnetism and Paleointensity of the 1.1 Ga Old Diabase Sheets from Central Arizona**

*Fabio Donadini*<sup>1</sup>, *Lauri J. Pesonen*<sup>2</sup>, *Kimmo Korhonen*<sup>3</sup>, *Alex Deutsch*<sup>4</sup> and *Stephen S. Harlan*<sup>5</sup>

<sup>1</sup>Institut für Geophysik, ETH Zürich, Sonneggstrasse 5, 8092 Zürich, Switzerland

<sup>2</sup>Division of Geophysics, University of Helsinki, Gustav Hällströmin Katu 2, 00014 Helsinki, Finland

<sup>3</sup>Geological Survey of Finland, Betonimiehenkuja 4, 02151 Espoo, Finland

<sup>4</sup>Institut für Planetologie, Westfälische Wilhelms-Universität Münster, Wilhelm Klemm-Str. 10, D-48149 Münster, Germany

<sup>5</sup>Department of Environmental Science and Policy, George Mason University, Fairfax, VA 22030-4444, USA

(Received: May 2010; Accepted: November 2010)

### *Abstract*

*Eighty-five oriented samples (33 sites) from diabase sheets (ca. 1100 Ma) were collected from Central Arizona. Detailed rock magnetic, petrological, paleomagnetic, and paleointensity analyses were performed. The rock magnetic studies, as well as thermal and alternating field demagnetization treatments of the specimens indicate that the primary natural remanent magnetization (NRM) is carried mainly by low-Ti magnetite. Other phases like maghemite are also present and are responsible for some of the secondary components.*

*In general paleomagnetic measurements isolate two distinct magnetic polarities, which show a clear asymmetry consistent with previous studies performed in Central Arizona as well as in the Grand Canyon and in the Lake Superior regions. Two of the sites in the present study also reveal directions that appear to be consistent with two distinct symmetric events.*

*The asymmetry, almost entirely in inclination, is of the same sense as the Lake Superior one, but appears larger with a very steep (upward) reversed inclination and a moderately shallow (downward) normal one. The normal component has a mean direction of  $D = 274.8^\circ$ ,  $I = 38.7^\circ$  ( $N = 13$  sites,  $k = 30.4$  and  $\alpha_{95} = 7.6^\circ$ ). The reversed AR2 component has a mean direction  $D = 193.7^\circ$ ,  $I = -78.7^\circ$  ( $N = 5$  sites,  $k = 24.7$  and  $\alpha_{95} = 15.7^\circ$ ). The angle between the two directions is about  $126^\circ$ , indicating an inclination offset of about  $30^\circ$ . The present study reveals at one site a steep downwards inclination (site DF,  $N=1$ ,  $D=332.6^\circ$ ,  $I=69.4^\circ$ ,  $k=145.5$ ,  $\alpha_{95} = 3.5^\circ$ ) that is antipodal to the reversed component. At another site (SD) we also observed a reversed component ( $N=1$ ,  $D=95.8^\circ$ ,  $I=-35.9^\circ$ ,  $k=60.7$ ,  $\alpha_{95} = 7.8^\circ$ ) that is antipodal to the normal component. Although further data showing these trends are required, the current set suggests that there may have been two symmetric reversal events, separated by a rapid apparent polar wander. A similar conclusion was drawn recently on a study of the Mamainse Point volcanic sequence (Swansson-Hysell et al., 2009).*

*The paleointensity results indicates that the field was weak during the emplacement of the dykes (normal polarities field:  $15.0 \pm 5.9 \mu\text{T}$ , reversed polarities field:  $9.5 \pm 5.5 \mu\text{T}$ ). Although the paleofield during the normal period appears higher than during the reversed one, the scatter in the mean values indicates that the two means are indistinguishable.*

*Key words: asymmetry reversal, Precambrian, Central Arizona diabases*

## 1. Introduction

Large Igneous Provinces (LIPs) represent times when huge volumes of mafic magma were emplaced in a relatively short period of time (*Ernst and Buchan, 2003*). One of the most dramatic LIP is the 1.12–1.06 Ga Keweenawan rift-related magmatism in the Lake Superior area of North America (NAM). This event is temporally related with the diabase province of the SW USA, and includes the Gila County and Sierra Ancha regions, as well as the Unkar Group in Grand Canyon (Arizona). In South Africa, the Umkondo mafic province in the Kaapvaal craton forms another LIP which has recently been temporally correlated with Keweenawan (Laurentia) magmatism on the basis of new U-Pb and magnetostratigraphic data (*Hanson et al., 2004*). The about 1.1 Ga magmatic activity has also taken place in the Grunehogna (e.g. *Powell et al., 2001*), and Coats Land (*Gose et al., 1997*) provinces of Antarctica. Less precisely dated, but probably related to the global 1.1 Ga mafic magmatism are the Bahia and San Salvador dykes of Amazonia, which have ages of about 1.09 and 1.02 Ga respectively (*D'Agrella et al., 1990, 2004*). In the Fennoscandian shield the Salla dyke pulse (1.12 Ga; *Salminen et al., 2009*) and the Laanila-Kautokeino-Karasjoki dyke swarm (1.06 Ga; *Mertanen et al., 1996*) express this LIP event. Possible coeval kimberlite magmatism has been recently reported in the Dharwar craton in India (*Kumar et al., 2007*).

These magmatic activities clearly represent extensional events. They roughly coincide with the Grenvillian (Laurentia and Baltica) and Natal-Namagua (Africa) collisional events related to the assembly of Rodinia supercontinent. However, the docking history of Laurentia with other Rodinia continents is paleomagnetically poorly defined due to significant inclination asymmetry between the normal (N) and reversed (R) polarities, observed e.g. in Keweenawan rocks (*Pesonen and Halls, 1983*; and references therein).

Previous studies have shown that the asymmetry of the reversal is merely in inclination data: declinations are nearly antiparallel whereas inclinations reveal a 30° offset.

Several mechanisms for the asymmetry have been suggested: (a) non averaged secular variation (*Ernst and Buchan, 1993*), (b) remagnetization processes (*Palmer, 1970*), (c) rapid motion of the North American plate during R to N crossing (*Pesonen and Halls, 1983*), and (d) strong non-dipole contribution of the Earth's magnetic field when the rocks got magnetized (*Pesonen and Nevanlinna, 1981*). Other hypotheses such as True Polar Wander (TPW; e.g. *Evans, 2003*) have also been suggested, but are not considered here. We also emphasize that analytical errors for absolute age data of more than 10 million years (see Table 1) may correspond to the time span for several reversal events. For example, *Swansson-Hysell et al. (2009)* show that the Mamainse Point volcanic sequence in Lake Superior consists of three distinct successive symmetric events.

Table 1. Age determinations available from diabases of the Gila County and Sierra Ancha areas (Central Arizona) and surroundings. Zircon (Zr) or baddeleyite (Bd) found as inclusions in garnet (Gr) or pegmatite (Peg), as well as biotite (Bt), or whole rock (WR) were used for isotope dating. Modified after *Harlan* (1993).

| No | Location                      | Method  | Material | Age [Ma]   | Reference  |
|----|-------------------------------|---------|----------|------------|--|
| 1  | Sierra Ancha diabase, AZ      | U - Pb  | Zr(Gr)   | 1075 ± 50  | Silver, 1960   |
| 2  | Sierra Ancha diabase, AZ      | U - Pb  | Zr(Gr)   | 1100 ± 30  | Silver, 1960, 1963                                       |
| 3  | Sierra Ancha diabase, AZ      | U - Pb  | Zr(Gr)   | 1120 ± 10  | Silver, 1978   |
| 4  | Sierra Ancha diabase, AZ      | U - Pb  | Zr, Bd   | 1100 ± 2   | Shastri et al., 1991<br>Damon et al., 1962; Wrucke, 1989 |
| 5  | Sierra Ancha diabase, AZ      | K - Ar  | Bt       | 1140 ± 30  |  |
| 6  | Miami diabase, AZ             | K - Ar  | Bt       | 1140 ± 40  | Banks et al., 1972                                       |
| 7  | Little Dragoon Mtn. Diabase   | Pb -Pb  | Zr(Peg)  | 1100 ± 15  | Silver, 1978   |
| 8  | Death Valley diabase, CA      | U - Pb  | Bd       | 1087 ± 3   | Heaman & Grotzinger, 1992                                |
| 9  | Death Valley diabase, CA      | U - Pb  | Bd       | 1069 ± 3   | Heaman & Grotzinger, 1992                                |
| 10 | Hualapai Mtn. diabase, AZ     | K - Ar  | WR       | 1070 ± 25  | Hammond and Wooden, 1990                                 |
| 11 | Grand Canyon diabase, AZ      | Rb - Sr | WR       | 1153 ± 30  | Hendricks, 1972  |
| 12 | Grand Canyon diabase, AZ      | Rb - Sr | WR       | 1070 ± 30  | Hendricks, 1972  |
| 13 | Grand Canyon diabase, AZ      | Rb - Sr | WR       | 1090 ± 90  | McKee & Noble, 1976                                      |
| 14 | Cardenas lavas, AZ            | Rb - Sr | WR       | 1070 ± 70  | Elston et al., 1982                                      |
| 15 | G. Canyon (Unkar) diabase, AZ | Ar - Ar | Bt       | 1090 ± 4.5 | Weil et al., 2003  |
| 16 | G. Canyon (Unkar) diabase, AZ | Ar - Ar | Bt       | 1104 ± 2   | Timmons et al., 2005                                     |
| 17 | Sierra Ancha granophyre*, AZ  | U - Pb  | Zr       | 1038 ± 11  | Spencer et al., 2003                                     |

Previous paleomagnetic studies of the ca. 1.15–1.00 Ga intrusions or baked rocks in the Central Arizona (*Elston*, pers. comm., 1987, *Helsley*, 1965, *Helsley and Spall*, 1972, *Sandberg and Butler*, 1986, *Harlan*, 1993) revealed in most cases strong asymmetric reversals (*Harlan*, 1992, 1993, *Elston et al.*, 2002). The N polarity data are in agreement with observations of the Keweenawan units around the Lake Superior region of North America (*Pesonen and Halls*, 1983, *Hnat et al.*, 2006, *Tauxe et al.*, 2010). However, the R polarity poles of Arizona plot distinctly away from R poles of the Lake Superior regions, thus suggesting an even larger asymmetry in Arizona (*Harlan*, 1993). In this study we performed paleomagnetic and paleointensity measurements of the central Arizona dykes to shed light on the asymmetry problem.

## 2. *Geology of the Central Arizona area*

The North American craton represents an ovoid shaped area with a diameter of about 5 000 km. It extends from Northern Canada to SW America. The ages of rocks represent almost the whole Precambrian era. The craton is encircled by younger Phanerozoic fold belts, and it is divided in seven main geological provinces, the Grenville one being the youngest with an age ranging between 1.3 and 1.1 Ga. The whole Grenville belt extends with a SW trend from Canada down to Mexico and is about 2 000 km long. The studied area (Central Arizona) is located in the transition zone between the Colorado Plateau and the Basin and Range Province (Fig. 1b).

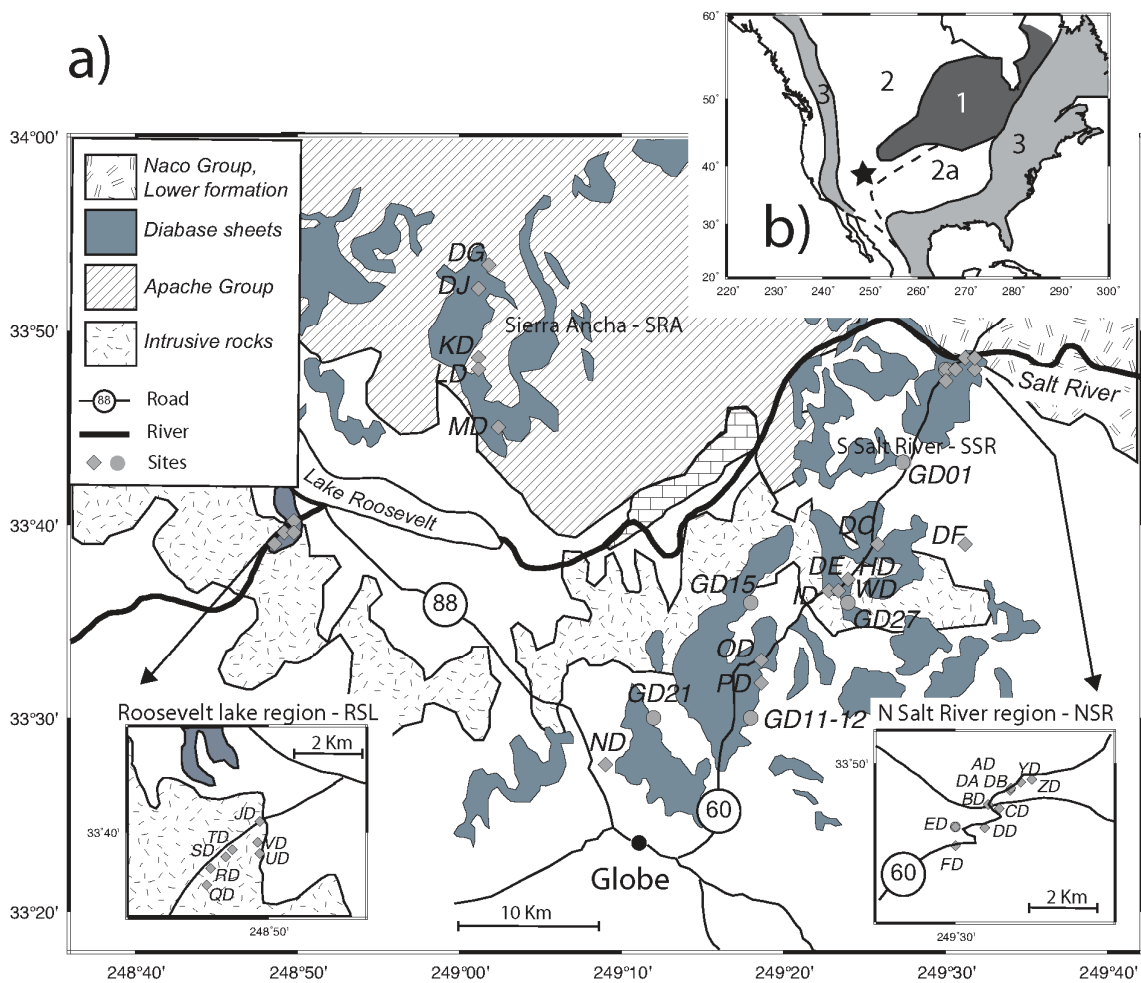


Fig. 1. a) Geological sketch map showing distribution of diabase exposures in the Gila County and Sierra Ancha regions, Central Arizona. Circles represent sampling sites of Harlan (1993), diamonds represent the sites of this study. b) Precambrian provinces in North America: 1) Superior and Wyoming (3.0 to 2.5 Ga), 2) Churchill (2.5 to 1.8 Ga), 2a) Central (1.8 to 1.4 Ga), and 3) Grenville (1.4 to 1.0 Ga). The star represents our study area. Ten minutes on the map correspond to 18 km.

The diabases, exposed as sills and dykes, are an expression of the North American large igneous province (LIP) that was emplaced about 1.1 Ga ago. These diabases intruded between 1153 to 1069 Ma ago (Table 1), and are found in the Gila County and Sierra Ancha regions in Central Arizona. They intrude beneath the Troy Quartzite formation and above the Mescal Limestone and Pioneer Shale formations, part of the Apache Group. They appear to correspond in age with the Cardenas lavas that intruded in Grand Canyon about 1104–1090 Ma ago (Weil *et al.*, 2003, Timmons *et al.*, 2005). Unfortunately, the ages are not associated to distinct polarities, however, if we take into account only ages with a  $2\sigma$  error less than 10 Ma, the diabase emplacement has occurred between 1169 and 1120 Ma.

The thickness of the diabase sheets varies in general between 1 and 30 m (Shride, 1967). However, depending on the level of erosion of the surrounding rocks, thinner diabases (ca. 15 cm) are also present. According to Howard (1991), the presence of granite bodies with no foliation lead to an horizontal to subhorizontal intrusion of the

dykes, because these granite bodies fracture more easily along the plane with least compression. For simplifying the visualization on Figure 1, we divided the study area into four regions: North of Salt River (NSR), South of Salt River (SSR), Roosevelt Lake (RSL), and Sierra Ancha (SRA).

As a whole, the whole area appears to have suffered minor ( $<5^\circ$ ) clockwise rotation relative to the stable plateau (Harlan, 1993; Steiner, 2003).

Locally, the diabases are altered and disintegrate to a brown clayish matrix. When fresh, the diabases look green-grayish, and are in general fine to medium grained. Petrologically the diabases are gabbros or monzonites (Shride, 1967; Nehru and Prinz, 1970; Smith, 1970; Banks and Krieger, 1977; Hammond, 1986; Wrucke, 1989) with plagioclase and clinopyroxene as major components, occasionally olivine, and magnetite, ilmenite, and various sulfides as accessory phases.

### 3. Methodology

Field campaigns were conducted during 2004 and 2005. In the field, three to fifteen oriented hand samples per site were collected from 33 sites. The orientation was performed using a magnetic compass, and IGRF declination at each site was evaluated to correct for geographic North. The compass was always kept at least 15cm away from the rock in order to avoid possible biases of the reading. All magnetic measurements were carried out at the laboratory for solid Earth geophysics of the University of Helsinki, Finland.

The magnetization of the diabases was determined using a superconducting DC-SQUID (2G) magnetometer, and an AGICO JR6-A spinner magnetometer. In general alternating field (AF) demagnetization up to 160 mT was employed to perform the directional analysis. In some cases, thermal demagnetization up to 680°C was also used. Principal component analysis to define the characteristic remanent magnetization component (ChRM) was performed using the PmagPY software of Tauxe *et al.* (2010).

Paleointensity measurements were performed using a Shonstedt TD1 oven and a laboratory field ( $B_{\text{lab}}$ ) of 50  $\mu\text{T}$ . The Coe method (Coe, 1967), with additional pTRM and pTRM tail checks (Riisager and Riisager, 2001) was selected for the intensity experiments. The samples were oriented in the oven so that the NRM was aligned with the applied laboratory field  $B_{\text{lab}}$ , in order to minimize the effects of TRM anisotropy (Gallet and LeGoff, 2006). Paleointensity analyses were performed with the Thellier Tool software of Leonhardt *et al.* (2004).

The hysteresis parameters were determined on each sample using a Princeton Measurements Corp. Vibrating Sample Magnetometer (VSM). Additionally, high temperature susceptibility curves and anisotropy of magnetic susceptibility (AMS) were determined with an Agico KLY-3a kappabridge. Basic petrophysical investigation was carried out using the Risto 5 petrophysics equipment, consisting of devices for low field susceptibility, remanence meter, mass, volume, and density measurements.

The petrological classification of the various dike lithologies was carried out mainly at the University of Münster using more than 20 thin sections of samples from

localities AD, CD, DA, ED, DE, GD, HD, JD, LD, MD, ND, OD, and PD (cf. Fig. 1) using optical and scanning electron microscopy (SEM). Another set of SEM analyses was performed at the Geological Survey of Finland, Espoo using a Jeol JSM-5900LV microscope. Separated magnetic particles were characterized (uncoated) with the field emission scanning electron microscope FE-SEM JEOL 6300F (Interdisziplinäres Centrum für Elektronenmikroskopie und Mikroanalyse [ICEM] University of Münster) operating at 5 kV acceleration voltage, and the crystal structure was identified/confirmed by X ray powder diffraction analyses (Inst. f. Mineralogie, University of Münster).

To constrain mineral chemistry in the specimens used for magnetic measurements, a set of thin sections was cut from site DA samples. The ore minerals in these samples were investigated by semi-quantitative energy-dispersive analysis (EDX) techniques using the SEM JEOL 840A (ICEM) operating at 20 kV acceleration voltage. Element mapping and mineral analysis of the ore minerals was done with the JEOL JXA 8600 MX Superprobe, Institut f. Mineralogie, University of Münster, operating at 15 kV acceleration voltage, using natural oxides as standards except for Ca (diopside), V (metal), Al (kyanite), and Mn (rhodonit).

All maps and part of the stereoplots were done using Generic Mapping Tools (*Wessel and Smith, 1991*).

#### 4. *Rock magnetic measurements*

Rock magnetic analyses were performed for each site. The data in Table 2 were divided according to polarities, to seek possible differences in magnetic properties. Site DF (N) and SD (R), denoted by an \*, are the two sites that appear to be antipodal to the typical steep upwards R polarity or moderately shallow downwards N polarity directions respectively (see next section). Mixed polarity sites (site DA) show both normal and reversed behaviour; whereas the *Rejected* sites are sites that did not pass the paleomagnetic reliability criteria. Three of the rejected sites (ND, XD, and VD; denoted by a \*\* in Table 2) were excluded based on rock magnetic or geological constrains: site ND has very high Q-values, site XD3 is not a diabase, and site VD is an outlier.

Weak field susceptibility and NRM intensity are scattered for both polarities, and reflect the various types of rock. We observe that susceptibility varies between 200 and  $100.000 \times 10^{-6}$  SI, whereas NRM varies between 10 and 10.000 mA/m (Fig. 2 and Table 2). Table 2 shows that there are no marked differences in density and susceptibility data of the four areas. The same observation applies to the two polarities (N and R). The Koenigsberger ratio (Q-value) of the diabases ranges between 0.9 and 3.0, with a mean value of 1.6 in case of N polarity. For reverse polarity samples, the Q values range between 0.3 and 1.6, and have a mean value of 1.3.

Table 2. Petrophysical properties of the different rock types (R.T.): diabase sheets (db), gabbros (gb), monzonites (mz), baked granites (b. gr.), baked sediments (b. s.), and felsic lavas (f. l.). Mean density ( $\rho$ ) [ $\text{kg/m}^3$ ], susceptibility ( $\kappa$ ) [ $10^{-6}\text{SI}$ ], natural remanent magnetization (NRM) [ $\text{mA/m}$ ], Koenigsberger ratio (Q), and the ratio between intensity after 20 mT demagnetizing treatment and NRM (J20/J0) are given for each site. Mean values include diabases, gabbros and monzonites, but not baked sediments. Sites denoted by \* appear to be antipodal to their reversed component, whereas sites denoted by a \*\*are excluded on the basis of rock magnetic or geological constrains.

| Site              | Lat   | Lon    | R.T.  | $\rho$      | $\kappa$     | NRM         | Q          | J20/J0     |
|-------------------|-------|--------|-------|-------------|--------------|-------------|------------|------------|
| Normal polarity   |       |        |       |             |              |             |            |            |
| AD                | 33,80 | 249,53 | db    | 2915        | 12125        | 685         | 2.5        | 0.6        |
| DB                | 33,80 | 249,51 | db    | 3084        | 126840       | 9116        | 1.8        | 1.3        |
| DC                | 33,65 | 249,43 | db    | 2982        | 18866        | 1573        | 2.0        | 0.5        |
| DF*               | 33,65 | 249,52 | db    | 2955        | 1852         | 157         | 1.9        | 0.9        |
| DG                | 33,89 | 249,03 | gb    | 2899        | 8967         | 735         | 2.0        | 0.1        |
| DJ                | 33,87 | 249,02 | db    | 2974        | 37173        | 1985        | 1.3        | 0.5        |
| ED                | 33,79 | 249,50 | db    | 2972        | 5080         | 608         | 3.0        | 0.3        |
| ED                | 33,79 | 249,50 | b. s. | 2713        | 1287         | 26          | 0.4        | 0.6        |
| FD                | 33,79 | 249,50 | db    | 2964        | 34916        | 1365        | 1.0        | 0.3        |
| GD                | 33,65 | 249,43 | gb    | 2997        | 18456        | 1000        | 1.3        | 0.3        |
| KD                | 33,81 | 249,02 | db    | 2919        | 19960        | 892         | 1.2        | 0.7        |
| LD                | 33,80 | 249,02 | db    | 2908        | 28472        | 1066        | 0.9        | 0.6        |
| MD                | 33,75 | 249,04 | db    | 2925        | 30200        | 1171        | 1.0        | 0.5        |
| OD                | 33,55 | 249,31 | mz    | 2962        | 72911        | 2278        | 0.8        | 0.3        |
| ZD                | 33,81 | 249,53 | gb    | 2962        | 28219        | 1395        | 1.2        | 0.3        |
| <b>mean</b>       |       |        |       | <b>2928</b> | <b>31717</b> | <b>1716</b> | <b>1.6</b> | <b>0.5</b> |
| <b>std</b>        |       |        |       | <b>47</b>   | <b>32572</b> | <b>2201</b> | <b>0.7</b> | <b>0.3</b> |
| Reversed polarity |       |        |       |             |              |             |            |            |
| BD                | 33,80 | 249,50 | db    | 2858        | 749          | 10          | 0.3        | 1.0        |
| BD                | 33,80 | 249,50 | b. s. | 2545        | 290          | 121         | 9.5        |            |
| CD                | 33,80 | 249,50 | db    | 2730        | 818          | 10          | 0.4        | 1.0        |
| DE                | 33,62 | 249,40 | db    | 2986        | 39031        | 1204        | 0.7        | 1.3        |
| ID                | 33,61 | 249,38 | db    | 3000        | 42562        | 2036        | 1.1        | 1.0        |
| WD                | 33,61 | 249,39 | db    | 2963        | 40081        | 2303        | 1.6        | 0.8        |
| SD*               | 33,66 | 248,82 | db    | 2986        | 25179        | 1306        | 1.2        | 0.3        |
| TD                | 33,66 | 248,82 | db    | 3000        | 28343        | 585         | 0.5        | 0.9        |
| <b>mean</b>       |       |        |       | <b>2928</b> | <b>25051</b> | <b>1061</b> | <b>1.3</b> | <b>0.8</b> |
| <b>std</b>        |       |        |       | <b>95</b>   | <b>16556</b> | <b>846</b>  | <b>0.5</b> | <b>0.4</b> |
| Mixed polarity    |       |        |       |             |              |             |            |            |
| DA                | 33,81 | 249,52 | mz    | 3022        | 55618        | 3292        | 1.3        | 0.9        |

Table 2. Continue.

| Site        | Lat   | Lon    | R.T.  | $\rho$      | $\kappa$     | NRM         | Q           | J20/J0     |
|-------------|-------|--------|-------|-------------|--------------|-------------|-------------|------------|
| Rejected    |       |        |       |             |              |             |             |            |
| DD          | 33,79 | 249,50 | db    | 2969        | 18116        | 4774        | 6.6         | 0.8        |
| HD          | 33,62 | 249,40 | db    | 2942        | 22663        | 757         | 1.0         | 0.5        |
| JD          | 33,67 | 248,83 | db    | 2961        | 34314        | 1363        | 1.0         | 0.9        |
| JD          | 33,67 | 248,83 | b. s. | 2344        | 244          | 30          | 7.6         | 0.9        |
| JD          | 33,67 | 248,83 | b. gr | 2572        | 307          | 462         | 37.0        | 1.0        |
| ND**        | 33,46 | 249,15 | db    | 2979        | 5210         | 1237        | 10.5        | 0.6        |
| PD          | 33,53 | 249,31 | gb    | 2975        | 69788        | 2671        | 0.9         | 0.5        |
| QD          | 33,65 | 248,81 | db    | 3004        | 34625        | 978         | 0.7         | 0.5        |
| QD          | 33,65 | 248,81 | mz    | 2688        | 12831        | 2182        | 4.0         | 0.5        |
| RD          | 33,66 | 248,82 | mz    | 2899        | 690          | 6           | 0.2         | 0.2        |
| UD          | 33,66 | 248,83 | db    | 2999        | 25538        | 1073        | 1.0         | 0.3        |
| VD**        | 33,66 | 248,83 | db    | 2899        | 23649        | 1038        | 1.3         | 0.3        |
| XD**        | 33,81 | 249,52 | f. l. | 2719        | 35653        | 9126        | 6.5         | 0.4        |
| YD          | 33,81 | 249,53 | db    | 2956        | 14075        | 16971       | 21.7        | 0.5        |
| <b>mean</b> |       |        |       | <b>2889</b> | <b>22818</b> | <b>3467</b> | <b>7.6</b>  | <b>0.6</b> |
| <b>std</b>  |       |        |       | <b>144</b>  | <b>19434</b> | <b>4936</b> | <b>11.1</b> | <b>0.2</b> |

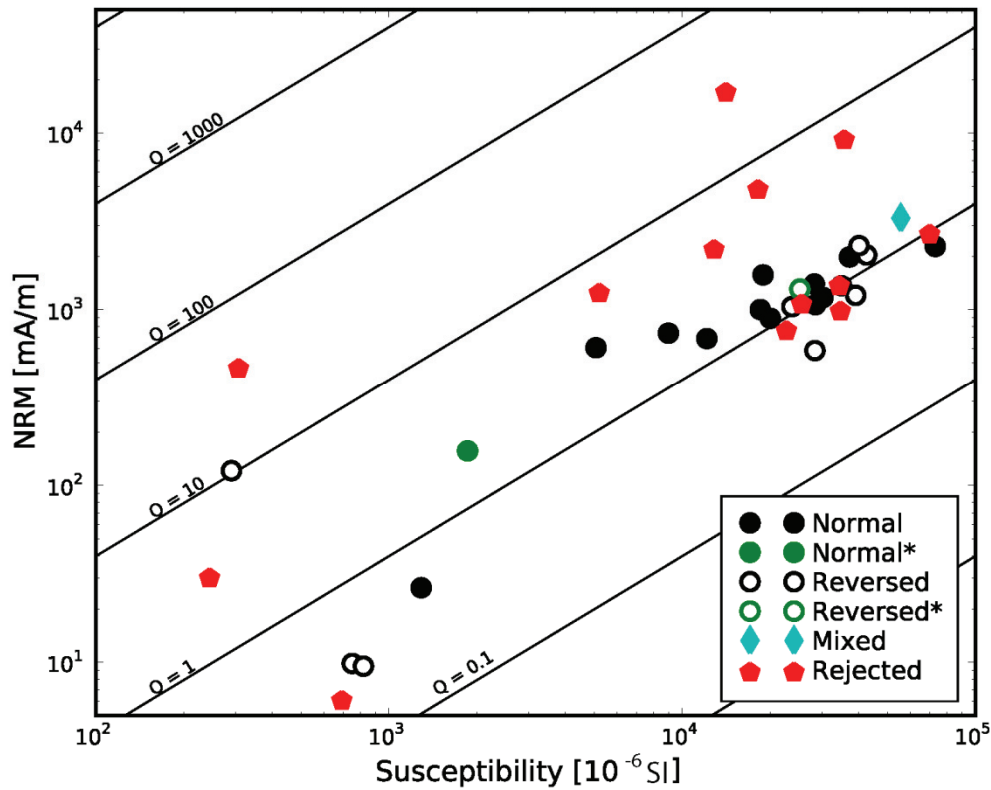


Fig. 2. Logarithmic plot of NRM versus susceptibility displayed as a mean for each site. N, R denote normal and reversed polarities, respectively. Mixed rocks show both N and R polarities. Normal\* and Reversed\* represent site DF and SD, respectively. Rejected sites are the paleomagnetically unstable. The Koenigsberger ratio (Q) for a 50 $\mu$ T field is also shown.

Table 3. Rock magnetic data for the different Central Arizona sites. Hysteresis parameters are defined as follows:  $M_S$  [ $\text{mAm}^2/\text{kg}$ ] is the saturation magnetization,  $M_R$  [ $\text{mAm}^2/\text{kg}$ ] is the remanent magnetization,  $H_C$  [mT] is the coercive field,  $H_{CR}$  [mT] is the coercivity of remanence. The mineralogical change is defined on the basis of the reversibility of the heating and cooling curves, whereas the Curie temperature  $T_C$  [ $^{\circ}\text{C}$ ] is obtained from the second derivative of the heating curve. Sites denoted by \* appear to be antipodal to their reversed component, whereas sites denoted by a \*\* are excluded on the basis of rock magnetic or geological constrains.

| Site              | R. T. | $T_C$         | Min. Ch. | $M_{RS}$ | $M_S$  | $H_C$ | $H_{CR}$ | $M_{RS}/M_S$ | $H_{CR}/H_C$ |
|-------------------|-------|---------------|----------|----------|--------|-------|----------|--------------|--------------|
| Normal polarity   |       |               |          |          |        |       |          |              |              |
| AD                | db    | 94; 574       | signif.  | 553.7    | 4960.0 | 10.4  | 23.2     | 0.11         | 2.22         |
| DB                | db    | 576; 620      | signif.  | 352.9    | 3274.0 | 8.9   | 22.0     | 0.11         | 2.47         |
| DC                | db    | 574; 620      | signif.  | 68.1     | 450.3  | 12.8  | 24.7     | 0.15         | 1.93         |
| DF*               | db    | 580; 673      | signif.  | 0.8      | 2.3    | 42.7  | 73.9     | 0.36         | 1.73         |
| DG                | db    | 554; 621      | signif.  | 61.1     | 431.0  | 11.0  | 25.9     | 0.14         | 2.36         |
| DJ                | db    | 571           | moder.   | 191.3    | 302.8  | 9.3   | 26.3     | 0.63         | 2.82         |
| ED                | db    | 571; 640      | signif.  | 25.4     | 49.1   | 15.0  | 18.7     | 0.52         | 1.25         |
| ED                | b. s. | 320; 570; 675 | signif.  | 0.0015   | 0.0250 | 7.0   | 26.5     | 0.06         | 3.77         |
| FD                | db    | 548; 578; 672 | signif.  | 8.8      | 29.3   | 10.9  | 31.6     | 0.30         | 2.91         |
| GD                | db    | 550           | signif.  | 153.6    | 1074.0 | 11.2  | 22.1     | 0.14         | 1.97         |
| KD                | db    | 557; 620      | signif.  | 64.3     | 645.6  | 7.8   | 17.7     | 0.10         | 2.27         |
| LD                | db    | 542; 580      | signif.  | 161.7    | 1582.0 | 9.9   | 22.9     | 0.10         | 2.32         |
| MD                | db    | 300; 573; 620 | signif.  | 227.7    | 850.9  | 17.7  | 39.3     | 0.27         | 2.22         |
| OD                | db    | 340; 563      | moder.   | 0.6      | 4.6    | 11.8  | 25.1     | 0.13         | 2.14         |
| ZD                | db    | 566           | signif.  | 95.1     | 451.6  | 10.1  | 24.5     | 0.21         | 2.44         |
| <b>mean</b>       |       |               |          |          |        |       |          | <b>0.23</b>  | <b>2.22</b>  |
| Reversed polarity |       |               |          |          |        |       |          |              |              |
| BD                | db    | 300; 580      | signif.  | 166.0    | 1170.0 | 18.0  | 46.9     | 0.14         | 2.60         |
| BD                | b. s. | 300; 580; 660 | signif.  | 0.2      | 165.4  | 1.2   | 64.7     | 0.001        | 55.76        |
| CD                | db    | 580; 620      | signif.  | 439.9    | 996.4  | 35.7  | 63.8     | 0.44         | 1.79         |
| DE                | db    | 335; 580      | signif.  | 317.1    | 695.2  | 24.4  | 53.5     | 0.45         | 2.19         |
| ID                | db    | 571           | signif.  | 523.8    | 2381.0 | 17.5  | 29.8     | 0.22         | 1.70         |
| SD*               | db    | 573; (680?)   | moder.   | 206.8    | 1217.0 | 14.7  | 26.4     | 0.17         | 1.79         |
| TD                | db    | 556           | moder.   | 351.1    | 1835.0 | 16.8  | 30.7     | 0.19         | 1.83         |
| WD                | db    | 560; 620      | moder.   | 0.4      | 1.2    | 15.1  | 31.3     | 0.31         | 2.07         |
| <b>mean</b>       |       |               |          |          |        |       |          | <b>0.31</b>  | <b>1.98</b>  |
| Mixed polarity    |       |               |          |          |        |       |          |              |              |
| DA                | db    | 356; 579; 615 | signif.  | 946.6    | 2210.0 | 56.2  | 86.1     | 0.43         | 1.53         |
| Rejected          |       |               |          |          |        |       |          |              |              |
| DD                | db    | 578; 620      | signif.  | 325.9    | 1217.0 | 21.6  | 34.5     | 0.27         | 1.60         |
| HD                | db    | 360; 565; 680 | signif.  | 57.6     | 110.1  | 43.2  | 81.5     | 0.52         | 1.89         |
| JD                | db    | 343; 564; 620 | signif.  | 977.8    | 3130.0 | 24.5  | 38.5     | 0.31         | 1.58         |
| JD                | b. s. | 580; 670      | signif.  | 1.7      | 10.5   | 51.0  | 271.3    | 0.16         | 5.32         |
| ND**              | db    | 354; 569      | signif.  | 23.9     | 195.4  | 15.9  | 32.9     | 0.12         | 2.07         |
| PD                | db    | 571           | not sig. | 0.3      | 3.4    | 8.5   | 21.5     | 0.10         | 2.53         |
| QD                | db    | 575; 620      | signif.  | 97.9     | 196.9  | 14.9  | 25.7     | 0.50         | 1.72         |
| RD                | db    | 596; 630      | signif.  | 0.4      | 204.0  | 2.2   | 55.0     | 0.002        | 25.13        |
| UD                | db    | 563           | moder.   | 272.9    | 423.1  | 16.5  | 30.0     | 0.65         | 1.81         |
| VD**              | db    | 560; 620      | moder.   | 0.4      | 1.2    | 15.1  | 31.3     | 0.31         | 2.07         |
| XD**              | f. l. | 541; 620      | moder.   | 133.0    | 556.3  | 10.1  | 32.2     | 0.24         | 3.20         |
| YD                | db    | 546; 620      | moder.   | 79.5     | 628.8  | 9.3   | 28.0     | 0.13         | 3.00         |
| <b>mean</b>       |       |               |          |          |        |       |          | <b>0.23</b>  | <b>4.80</b>  |

High temperature susceptibility curves (Fig. 3), hysteresis loops (Fig. 4), and isothermal remanent magnetization (IRM) were determined on 62 specimens (Table 3). The data show that the main carrier of remanence is low-Ti magnetite (Curie temperature  $T_C$  between 540 and 580°C), consistent with the results of previous workers (Harlan, 1992, 1993). In some cases other magnetic phases are observed and correspond probably to maghemite ( $T_C= 300\text{--}350^\circ\text{C}$ ) and hematite ( $T_C= 620\text{--}680^\circ\text{C}$ ). Most of the samples show irreversible  $\kappa$  vs. T curves, suggesting that alteration processes occur during the thermal treatment (Fig. 3). Hysteresis loops show a relatively soft behaviour (Fig. 4), suggesting that pseudo single domain (PSD) to multidomain (MD) magnetite grains are the main carriers. In some cases (sites LD and QD) wasp-waisted loops can be observed, indicating that both low and high coercivity phases are present.

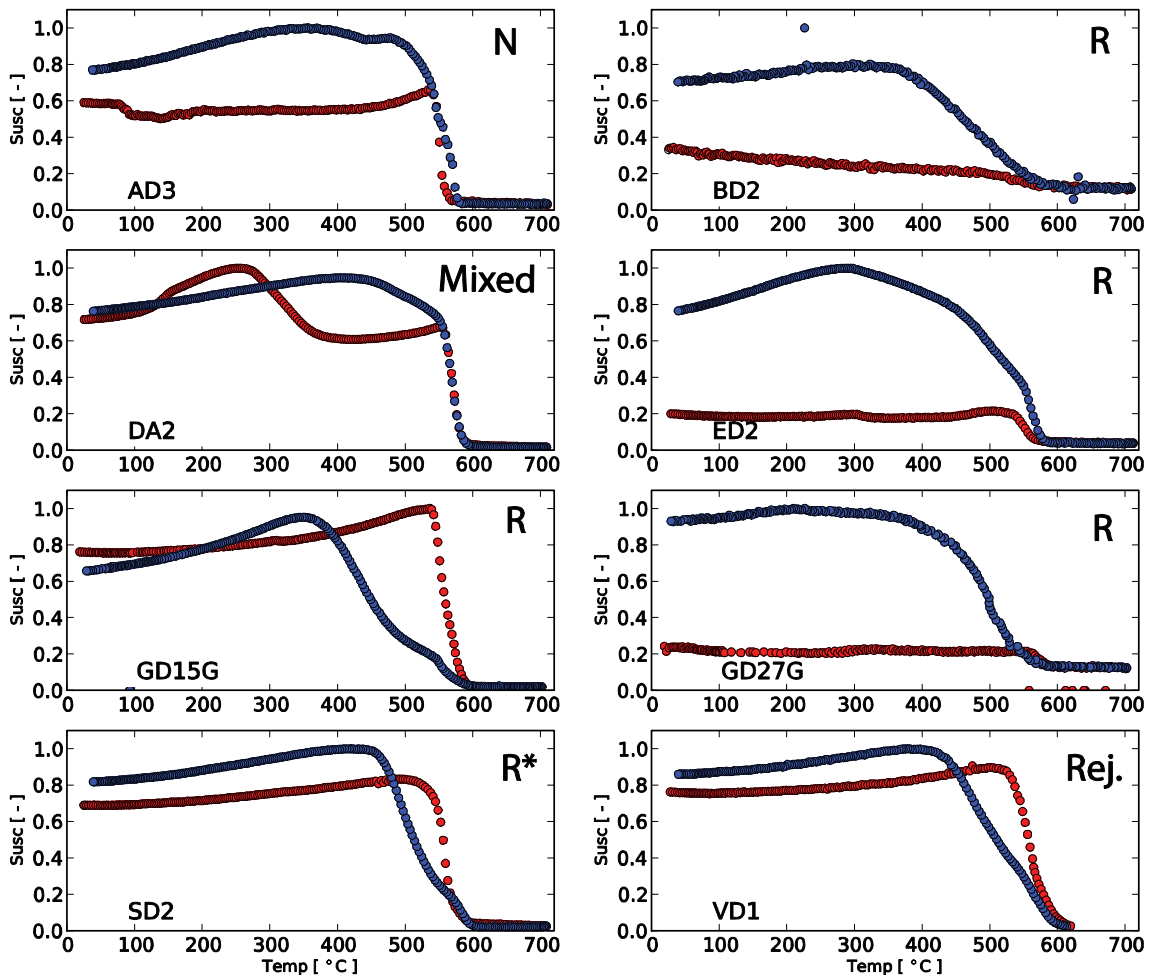


Fig. 3. Examples of susceptibility vs. temperature behaviors of samples from sites AD3 (N), BD2 (R), DA2 (Mixed), ED2 (R), GD15 (R, paleointensity), GD27 (R, paleointensity), SD2 (Reversed\*), VD1 (Rejected). Red (blue) line denotes heating (cooling). What is ARI?

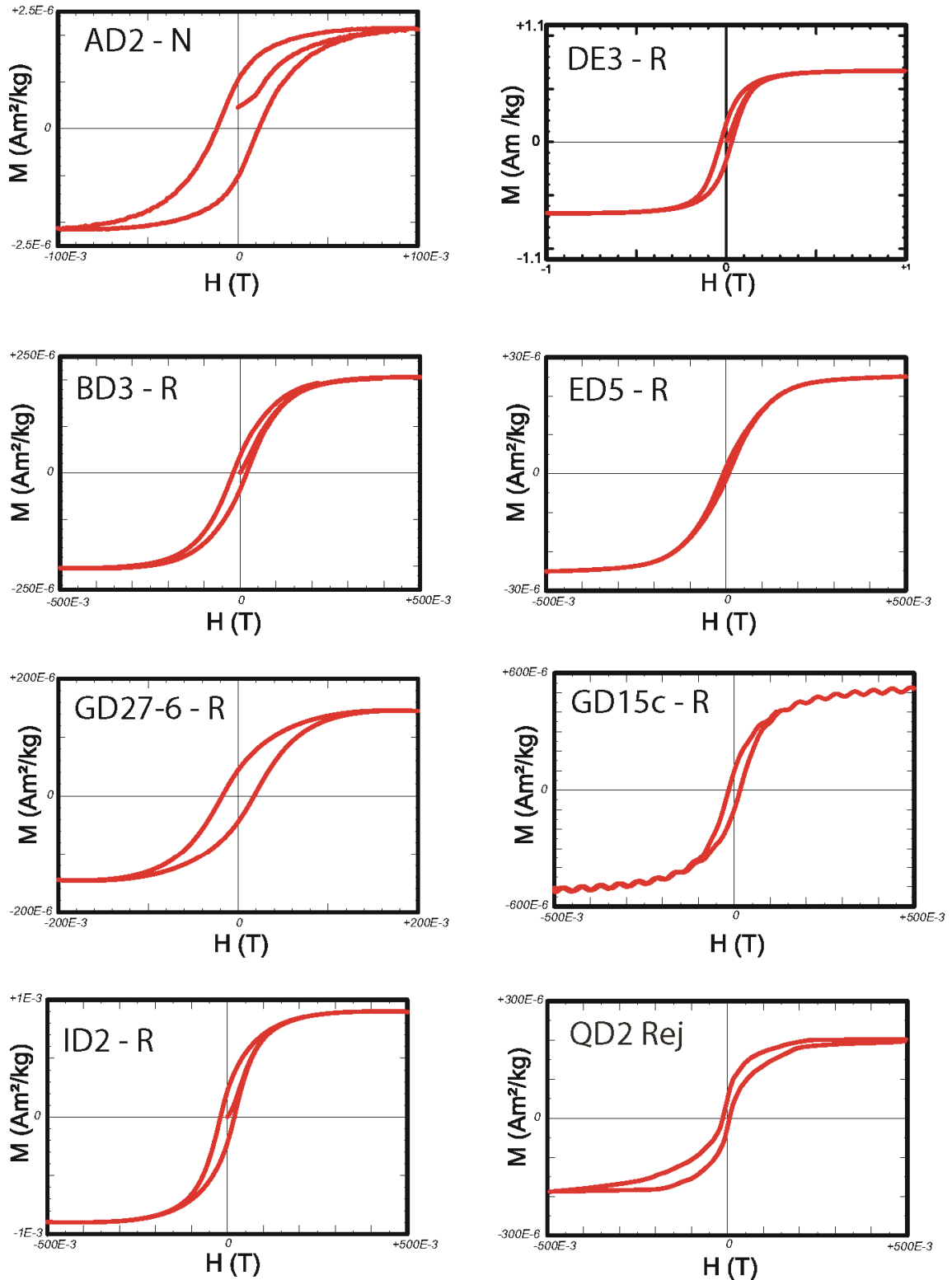


Fig. 4. Examples of hysteresis loops from sites AD2 (N), DE3 (R), BD3 (R), ED5 (R), GD27-6 (R, paleointensity), GD15c (R, paleointensity), ID2 (R), VD3 (Rejected).

The Day plot of hysteresis data (*Day et al.*, 1977; Fig. 5) shows that the phases relate mainly to PSD magnetite grains. Taking into account the Day-plot re-appraisal after *Dunlop* (2002), we notice that most of the normal polarity samples fall at the MD-SD mixing line. A few exceptions show variable content of superparamagnetic (SP)

compounds and one single domain (SD) case. On the other hand, the reversed data are somewhat more scattered in the Day plot, but on average we can observe the same hysteresis characteristics for both polarities. This is in accordance with the petrophysical data. Some of the rejected sites show higher values of  $H_{CR}/H_C$ , and point to mixtures of SD and SP grains.

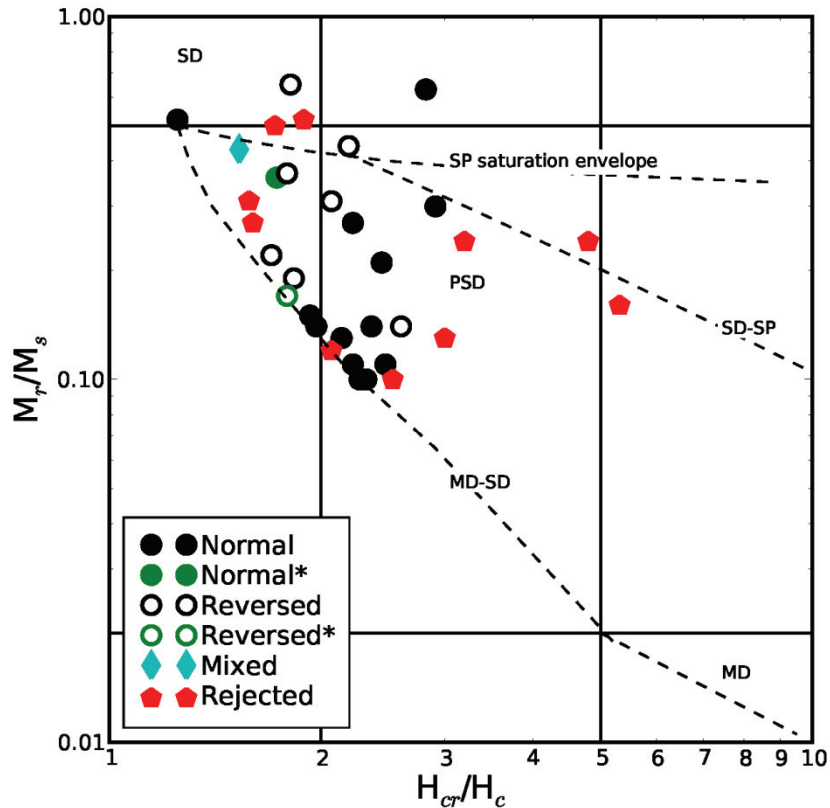


Fig. 5. Day plot of the investigated sites. See Figure 2 for explanations.

Anisotropy of magnetic susceptibility (AMS) was investigated on selected samples in order to see if the diabases record a specific orientation pattern of the magnetic grains (fabric), which could either indicate tectonism or preferred magma flow direction. The data are presented in Figure 6, and are presented as a cumulative distribution of the AMS eigenvector bootstrapped from a set of 23 N data and 9 R data, respectively (Tauxe, 2010). The figure indicates that in case of N polarity the three eigenvalues are different at 95% confidence interval (denoted by the vertical lines) whereas R polarities show some degree of overlap, and so the N polarities appear to be triaxial ( $K_1 > K_2 > K_3$ ), whereas R polarities are oblate ( $K_1 = K_2 > K_3$ ).

The main ore minerals in the Arizona diabase samples are ilmenite, magnetite, and minor quantities of pyrite, chalcopyrite, and sphalerite. The SEM study shows that textures are quite complicated and variable.

In one group of samples (e.g., sites ID, TL, WD, AD03, CD02, CD03, DD) the ilmenites are large ( $< 200 \mu\text{m}$ ) skeletal crystals, while the size of magnetite grains is less than  $5 \mu\text{m}$ , thus, in the PSD-SD domain grain sizes.

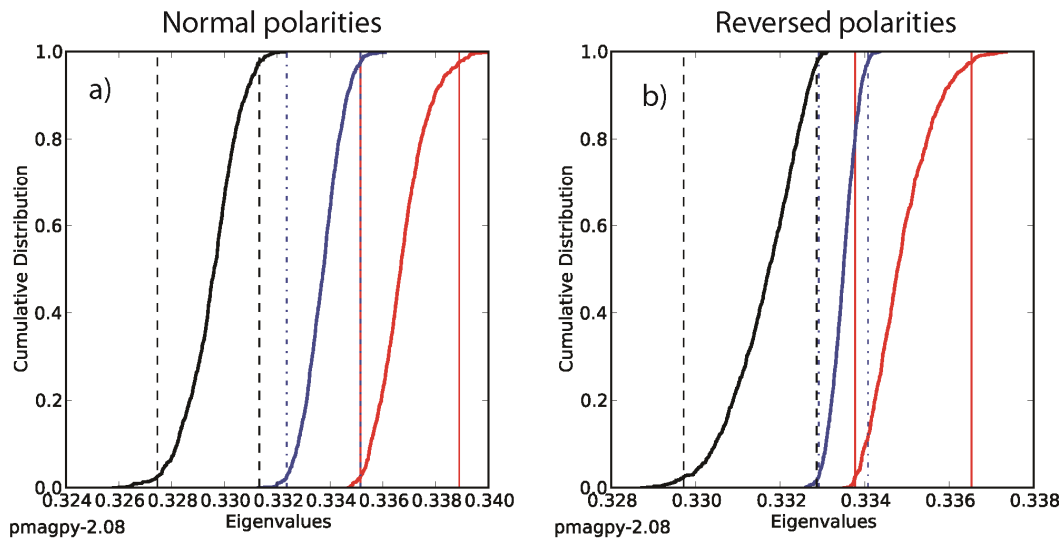


Fig. 6. Cumulative distribution of the AMS eigenvectors, calculated as a bootstrap analysis of 23 N specimens (a), and 9 R specimens (b). After *Tauxe et al.* (2010). Black, blue, and red colors represent the three eigenvectors K1, K2, and K3. Vertical lines presents the 95% confidence intervals.

Another group of diabase samples, e.g., DA1, 2, and 3, is characterized by lamellar intergrowths of ilmenite – magnetite (Fig. 7) and exsolutions on the  $\mu\text{m}$  to sub- $\mu\text{m}$  scale. It is worth noting that the samples from the DA site, showing distinct normal and reversed polarities, do not display significant differences in mineralogy.

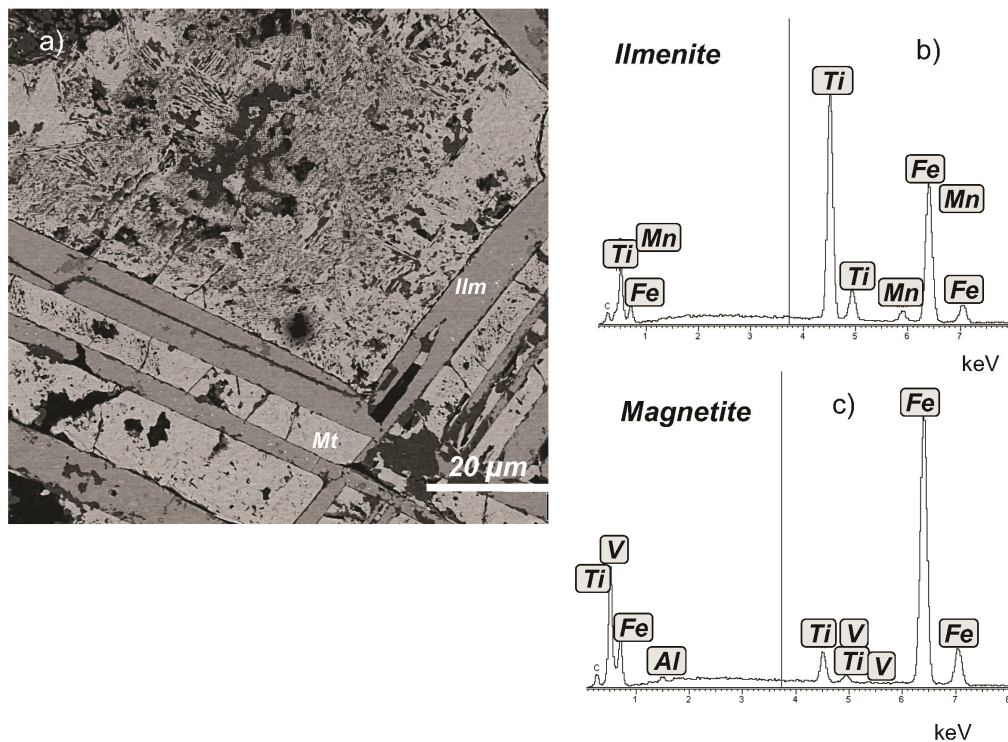


Fig. 7. a) Alternating lamellae of ilmenite (Ilm, dark grey) and magnetite (Mt, light steel grey) with interstitial finest-grained exsolution textures. b,c) The energy dispersive spectra (relative counts vs. energy) illustrate that both phases can be clearly distinguished on the base of semi-quantitative analyses. Important cations are Mn in the ilmente, and Ti, Al, and V in different proportions in the magnetite. Sample DA1-1; SEMJEOL840A, WWU Münster.

Microprobe results (Table 4) indicate that the magnetite contains various amounts of an ulvöspinel component, reaching in part up to 5.6 mol. %. Other components in solid solution are hercynite (<10 mol. %), and a spinel with V<sup>3+</sup> in the octahedral position (<2.1 mol. %). The analyzed ilmenites all carry a pyrophanite component (corresponding to about 2.3 wt. % MnO); the crystals are not fully stoichiometric, and the small calculated excess Fe<sub>2</sub>O<sub>3</sub> content may be either in solid solution or forms sub- $\mu$ -meter-sized small haematite inclusions.

Table 4. Chemical composition of selected ore minerals.

| sample<br>wt. %                  | DA1-1A             | DA2-1A               |                     | DA3-2A               |                     |
|----------------------------------|--------------------|----------------------|---------------------|----------------------|---------------------|
|                                  | mt #8 <sup>a</sup> | ilm #15 <sup>b</sup> | mt #16 <sup>a</sup> | ilm #20 <sup>b</sup> | mt #18 <sup>a</sup> |
| SiO <sub>2</sub>                 | 0.28               | <i>leq</i> 0.01      | 0.56                | 0.05                 | 0.11                |
| TiO <sub>2</sub>                 | 1.69               | 49.68                | 1.33                | 49.4                 | 6.84                |
| Al <sub>2</sub> O <sub>3</sub>   | 0.61               | n.d.                 | 0.32                | 0.08                 | 2.74                |
| V <sub>2</sub> O <sub>3</sub>    | 0.95               | n.d.                 | 0.53                | 0.81                 | 0.76                |
| Cr <sub>2</sub> O <sub>3</sub>   | n.d.               | 0.58                 | 0.27                | n.d.                 | 0.58                |
| Fe <sub>2</sub> O <sub>3</sub> * | 63.24              | 2.71                 | 64.13               | 4.21                 | 53.11               |
| FeO*                             | 31.96              | 42.53                | 29.6                | 41.23                | 33.44               |
| MnO                              | 0.12               | 2.28                 | 0.14                | 2.3                  | 0.3                 |
| MgO                              | <i>leq</i> 0.02    | <i>leq</i> 0.02      | 0.13                | 0.08                 | 0.05                |
| CaO                              | 0.17               | 0.18                 | 0.46                | 0.04                 | 0.03                |
| Total*                           | 99.19              | 97.99                | 97.49               | 98.19                | 97.95               |
| Si                               | 0.093              | --                   | 0.17                | 0.003                | 0.038               |
| Ti                               | 0.39               | 1.935                | 0.322               | 1.925                | 1.203               |
| Al                               | 0.269              | --                   | 0.113               | 0.006                | 1.005               |
| V                                | 0.27               | --                   | 0.152               | 0.031                | 0.186               |
| Cr                               | --                 | 0.025                | 0.076               | --                   | 0.149               |
| Fe+3                             | 14.723             | 0.158                | 15.339              | 0.168                | 12.319              |
| Fe+2                             | 8.273              | 1.842                | 7.906               | 1.835                | 8.66                |
| Mn                               | 0.018              | 0.081                | 0.375               | 0.081                | 0.005               |
| Mg                               | --                 | 0.003                | 0.057               | 0.006                | 0.019               |
| Ca                               | 0.056              | 0.009                | 0.152               | 0.00                 | 0.019               |

a) Structural formulae O=32

b) Structural formulae O=6

mt = magnetite; ilm = ilmenite; \* = calculated; n.d. = not detected

EMP analyses, see text for analytical details and explanations

## 5. Paleomagnetic results

In total, 266 specimens were AF demagnetized, and 55 specimens were selected for thermal treatment. Ten specimens were demagnetized using the low temperature demagnetization (LTD) as explained by *Borradaile et al.* (2004). We notice that the directions obtained by LTD are consistent with that ones obtained by standard AF treatment. Principal component analysis (PCA) reveals two distinct polarities: one with moderate inclination downwards and another one with steep inclination upwards. The former, hereafter called Az N, has westerly or north-westerly declination. The latter (Az

R), has a large variation in declination (SW to S-SE), as also observed in previous studies (Harlan, 1993; Sandberg and Butler, 1986), and might be justified by the very steep inclinations. For the final paleomagnetic analysis, we selected only samples that did show stable directions, and adopted a set of reliability criteria as follows: specimen  $MAD < 15^\circ$ , site  $\alpha_{95} < 15^\circ$  and  $k > 30$ , with at least 4 samples per site. In general we adopted the hierarchical approach (specimens are averaged into samples first, and then samples are averaged into sites) because it reduces the errors due to sampling. Unfortunately, several R specimens did not pass the criteria, and so we decided to average all of them into one final site mean. We did that because we observe that the scatter between samples is minimal.

Table 5. Representative paleomagnetic results of normal and reverse polarity sites at Gila County, Arizona. Site means are calculated as an average of all specimens measured. NI and Np represent the number of specimens calculated as a best-fit line and as a plane, respectively. Dec. and Inc. are the declination and inclination of the ChRM, with precision parameter k and 95% confidence angle  $\alpha_{95}$ . P<sub>lat</sub>, P<sub>lon</sub> represent the calculated Virtual Geomagnetic Pole latitude and longitude (not corrected here for 5° rotation of the Colorado plateau). Site denoted by \* (DF and SD) have antipodal directions to the components calculated here. Sites denoted by a \*\* are rejected based on geological and rock magnetic constraints. These sites are shown in *italic* and are not included in the mean.

| Site              | Dec.         | Inc.         | NI            | Np       | k             | $\alpha_{95}$ | PLat        | PLong        |
|-------------------|--------------|--------------|---------------|----------|---------------|---------------|-------------|--------------|
| Normal polarity   |              |              |               |          |               |               |             |              |
| AD                | 272.9        | 47.3         | 23            | 0        | 71.9          | 3.6           | 17.5        | 172.1        |
| DB                | 282.5        | 24.8         | 10            | 0        | 215.6         | 3.3           | 17.5        | 153.4        |
| DC                | 281.2        | 33.8         | 9             | 0        | 91.9          | 5.4           | 19.2        | 159.1        |
| <i>DF*</i>        | <i>332.6</i> | <i>69.4</i>  | <i>13</i>     | <i>0</i> | <i>145.1</i>  | <i>3.5</i>    | <i>62.4</i> | <i>202.5</i> |
| DG                | 266.2        | 34.4         | 6             | 1        | 58.7          | 8             | 7.3         | 167          |
| DJ                | 281.9        | 52.8         | 9             | 0        | 325.5         | 2.9           | 26.6        | 173.1        |
| ED                | 288.6        | 51.6         | 11            | 0        | 71.5          | 5.4           | 31.3        | 169.4        |
| FD                | 279.2        | 49.3         | 8             | 0        | 48.5          | 8             | 23.1        | 171          |
| GD                | 278.8        | 29           | 7             | 0        | 102.8         | 6             | 15.7        | 157.6        |
| KD                | 293.8        | 13.4         | 14            | 0        | 142.3         | 3.3           | 23.5        | 141.5        |
| LD                | 283.4        | 18.8         | 4             | 0        | 45.4          | 13.8          | 16.4        | 150          |
| MD                | 277.2        | 50.7         | 12            | 0        | 110.4         | 4.2           | 22.1        | 173.1        |
| <i>ND**</i>       | <i>341.2</i> | <i>40.4</i>  | <i>4</i>      | <i>0</i> | <i>80.9</i>   | <i>10.3</i>   | <i>70.5</i> | <i>121.7</i> |
| OD                | 276.8        | 50.1         | 13            | 0        | 64.5          | 5.2           | 21.6        | 172.7        |
| ZD                | 270.5        | 42.9         | 12            | 0        | 52.1          | 6.1           | 13.8        | 170.1        |
| <b>mean</b>       | <b>279.8</b> | <b>38.7</b>  | <b>13/139</b> |          | <b>30.4</b>   | <b>7.6</b>    | <b>19.7</b> | <b>172.8</b> |
| Reversed polarity |              |              |               |          |               |               |             |              |
| BD                | 137.6        | -74          | 2             | 5        | 66.1          | 8.2           | 51.7        | 186.4        |
| CD                | 138.8        | -75.2        | 8             | 3        | 33.4          | 8.1           | 51.4        | 189.6        |
| DE                | 292.1        | -74.8        | 4             | 0        | 359.9         | 4.8           | 19.6        | 267.2        |
| ID                | 226.7        | -65          | 9             | 0        | 52.2          | 7.2           | 52.5        | 293.8        |
| <i>SD*</i>        | <i>95.8</i>  | <i>-35.9</i> | <i>7</i>      | <i>0</i> | <i>60.7</i>   | <i>7.8</i>    | <i>15.5</i> | <i>163.0</i> |
| <i>VD**</i>       | <i>355.9</i> | <i>-31.5</i> | <i>5</i>      | <i>0</i> | <i>180.5</i>  | <i>5.7</i>    | <i>39.3</i> | <i>244.2</i> |
| <i>WD</i>         | <i>199.2</i> | <i>-71</i>   | <i>24</i>     | <i>0</i> | <i>92.1</i>   | <i>3.1</i>    | <i>64.3</i> | <i>264.6</i> |
| <i>XD3**</i>      | <i>173.2</i> | <i>-55</i>   | <i>0</i>      | <i>4</i> | <i>3034.8</i> | <i>3.2</i>    | <i>84</i>   | <i>171</i>   |
| <b>mean</b>       | <b>198.7</b> | <b>-78.7</b> | <b>5/55</b>   |          | <b>24.7</b>   | <b>15.7</b>   | <b>53.6</b> | <b>260.7</b> |

We adopt the correction proposed by *Harlan (1993)* and *Sandberg and Butler (1986)*, suggesting that the terranes have been coherently affected by a minor (about 5° clockwise) rotation around the vertical axis (rot. corr. in Table 5) during the Laramide orogeny.

Figure 8 shows examples of Zijderveld plots, stereographic (equal area) projections, and demagnetization curves of the isolated components for selected AF and thermal treatments.

In general a single component ChRM can be isolated after 10–20 mT AF demagnetizing field, which removes viscous magnetizations, presumably due to present Earth's magnetic field. In some cases, evidences of another secondary remanent magnetization can also be observed, and may originate from events that occurred during the Laramide orogeny (e.g. *Harlan, 1993*).

A typical example of N polarity direction is represented by sample AD5-1a (NSR, Fig. 8a). The N component is typically nicely isolated from low AF field values and is stable up to 160 mT, with exception of RSL region, where only thermal treatment appeared to be effective to isolate the ChRM.

A typical example of R polarity is represented by sample WD7-2a (SSR, Fig. 8b). The thermal treatment of this sample indicates that the ChRM is isolated between 480 and 580°C, and suggests that the remanence is carried by magnetite.

Site BD (a 10 cm wide dyke, in the gorge of Salt River Canyon) shows a reversed component at high AF demagnetizing fields (130–160 mT). The best way of isolating this component is adopting great circles (Fig. 8e). This same component also unblocks between 250 and 380°C (Fig. 8f), and is probably associated with maghemite. The reversed component of site BD is in good agreement with the mean R component. Additionally, site BD carries in general a N polarity component with SW declination and moderate inclination (about 240°, 40°), which unblocks between 500 and 580°C. It is not shown in Table 5 as it didn't pass the criteria for a reliable component.

At site DA both N and R polarities can be observed in different samples. Also in this case the high temperature susceptibility curve reveals three different magnetic phases: maghemite, magnetite and hematite. In this case the N component was isolated from sample DA3 (Fig. 8g). Samples DA1 and DA2 (Fig. 8h) are characterized by a reversed component which is in agreement with the mean R direction for the other diabases, and can be isolated with thermal method between 390 and 610°C, or between 20 and 160 mT using AF treatment. Unfortunately the results from this site do not pass the criteria, and so are not included in the final mean.

Site DF (Fig. 8c), from the NSR region, shows a particularly steep downward inclination. This seems to be an atypical N polarity sheet in the Central Arizona area, and is symmetric with the R polarity data. The direction for this site is isolated thermally between 200 and 580°C, or as a unique, single hard component when using AF method. Similarly, site SD (Fig. 8d), reveals a reversed component that is antipodal to the typical moderate shallow N polarity data. Its remanence deblocks between 500 and 580°C indicating that it is carried by magnetite.

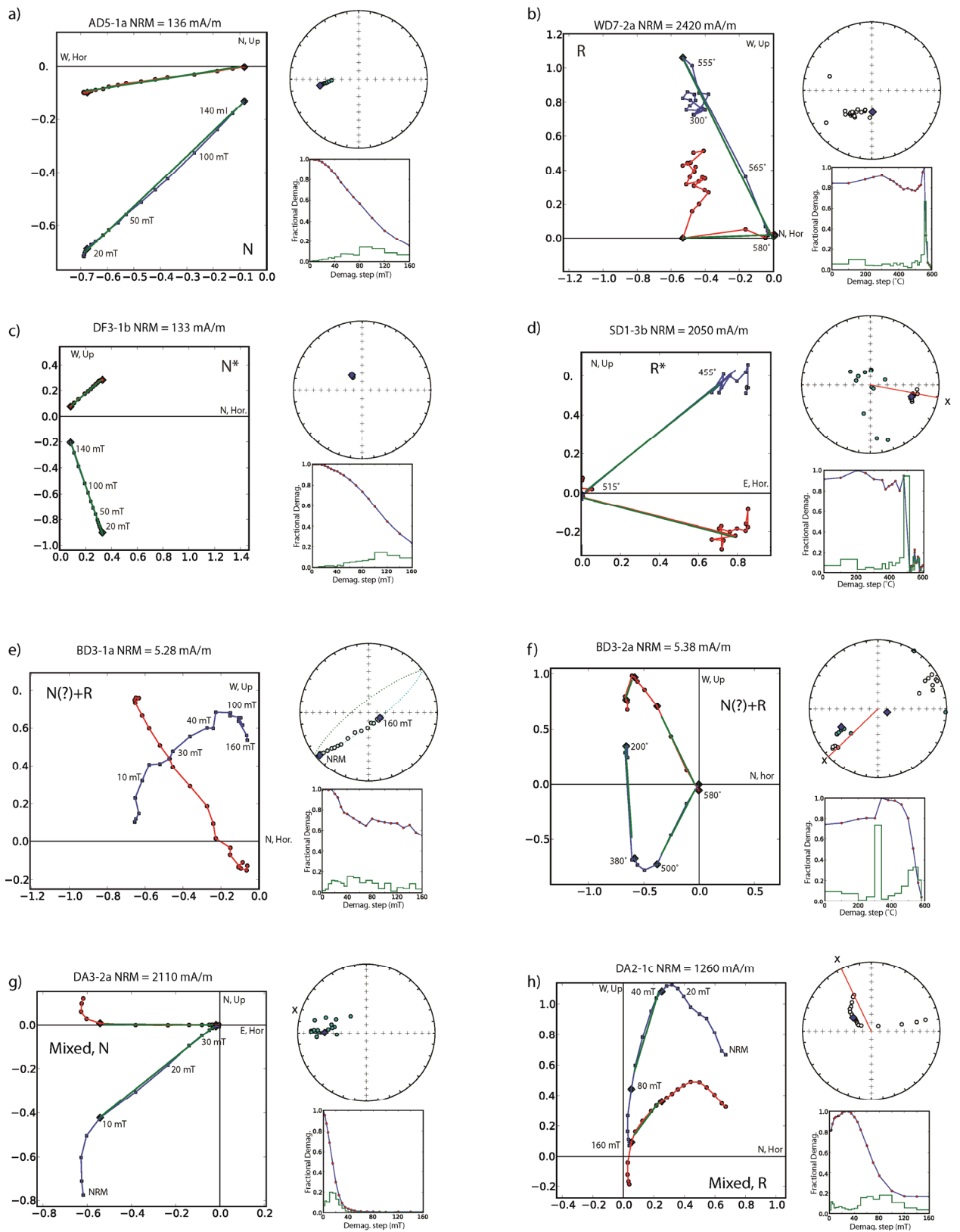


Fig. 8. Examples of paleomagnetic results from the Arizona diabase sheets. For each specimen a)-h) a Zijderveld plot (left), an equal area stereonet (upper right), and the demagnetization plot (lower right) are shown. In the Zijderveld plot, circles represent declination, whereas squares represent inclination.

In general the Central Arizona igneous diabase sheets are characterized by two distinct components, one with moderate downward inclination (Az N), and another one with steep upwards inclination (Az R). The paleomagnetic results appear to be in agreement with the previous studies performed in the area (*Helsley, 1965; Helsley and Spall, 1972; Sandberg and Butler, 1986; Harlan, 1993*) suggesting the occurrence of asymmetric reversals. However, two sites (DF and SD) hint to two symmetric events: site DF is antipodal to the Az R event, whereas site SD is antipodal to the Az N event.

## 6. Paleointensity results

Forty-six samples from a previous collection by *Harlan (1993)*; all GD samples) were used to determine the intensity of the Earth's magnetic field at the paleolatitude of Arizona. Additionally, 24 samples from this study were added. Reliability criteria were set as follows: pTRM checks < 10%,  $f > 0.3$ ,  $q > 2$ ,  $\alpha_{95} < 10^\circ$ .

Unfortunately, even with these loose criteria, most specimens failed to fulfill all criteria when heated within the unblocking temperature range (500–580°C), and so only 13 specimens were accepted. Table 6 shows the paleointensity determined from 9 N polarity sites as well as the intensity obtained from 4 R polarity sites; some representative results are presented in Fig. 9. The intensity of N polarity sheets (mean:  $15.0 \pm 5.9 \mu\text{T}$ ) and R ones (mean:  $9.5 \pm 5.5 \mu\text{T}$ ) are indistinguishable, and correspond to a mean VDM of  $2.5 \pm 1.0 \times 10^{22} \text{ Am}^2$  and  $1.4 \pm 1.0 \times 10^{22} \text{ Am}^2$  respectively.

Table 6. Paleointensity results for normal and reversed sites of the Gila County area, showing the ancient field ( $B_a$ ) and its standard deviation ( $\sigma B_a$ ), the temperature interval used to determine the paleointensity, the  $f$  and  $q$  factors, the associated directions as well as the corresponding VDM and VADM values. Samples marked with asterisks yielded reliable paleointensities, but have been rejected because the paleodirection does not match the site mean direction. Samples GD belong to *Harlan (1993)* collection.

| Specimen          | $B_a$<br>[ $\mu\text{T}$ ] | $\sigma B_a$<br>[ $\mu\text{T}$ ] | $T_{\min}$<br>[ $^\circ\text{C}$ ] | $T_{\max}$<br>[ $^\circ\text{C}$ ] | $f$ | $q$ | $D$<br>[ $^\circ$ ] | $I$<br>[ $^\circ$ ] | $\alpha_{95}$<br>[ $^\circ$ ] | VADM<br>[ $10^{22} \text{ Am}^2$ ] | $\sigma\text{VADM}$<br>[ $10^{22} \text{ Am}^2$ ] | VDM<br>[ $10^{22} \text{ Am}^2$ ] | $\sigma\text{VDM}$<br>[ $10^{22} \text{ Am}^2$ ] |
|-------------------|----------------------------|-----------------------------------|------------------------------------|------------------------------------|-----|-----|---------------------|---------------------|-------------------------------|------------------------------------|---|-----------------------------------|--|
| Normal polarity   |                            |                                   |                                    |                                    |     |     |                     |                     |                               |                                    |   |                                   |  |
| GD1-1a            | 24.5                       | 1.9                               | 20                                 | 500                                | 0.5 | 4.3 | 295.2               | 44.2                | 10.7                          | 5.0                                | 0.4   | 4.0                               | 0.3  |
| GD1-2a            | 21.0                       | 2.1                               | 20                                 | 500                                | 0.4 | 3.5 | 285.5               | 28.1                | 7.4                           | 4.3                                | 0.4   | 4.2                               | 0.4  |
| GD1i              | 13.2                       | 1.8                               | 300                                | 530                                | 0.4 | 3.3 | 277.7               | 30.7                | 3.0                           | 2.7                                | 0.4   | 2.6                               | 0.3  |
| GD1b              | 14.3                       | 1.9                               | 480                                | 540                                | 0.4 | 1.9 | 282.0               | 57.5                | 4.0                           | 2.9                                | 0.4   | 2.1                               | 0.3  |
| GD4b              | 21.7                       | 1.4                               | 430                                | 550                                | 0.2 | 3.0 | 279.2               | 46.0                | 3.1                           | 4.4                                | 0.3   | 3.5                               | 0.2  |
| GD24Ca            | 10.5                       | 1.3                               | 20                                 | 530                                | 0.3 | 2.6 | 281.6               | 44.3                | 1.6                           | 2.1                                | 0.3   | 1.7                               | 0.2  |
| GD24Fa            | 9.7                        | 1.2                               | 20                                 | 540                                | 0.3 | 3.1 | 273.0               | 33.7                | 6.1                           | 2.0                                | 0.2   | 1.8                               | 0.2  |
| GD23e             | 8.0                        | 0.6                               | 510                                | 570                                | 0.7 | 8.0 | 283.0               | -2.9                | 9.7                           | 1.6                                | 0.1   | 2.1                               | 0.1  |
| GD23i             | 12.1                       | 0.9                               | 490                                | 530                                | 0.5 | 4.8 | 293.5               | 11.4                | 2.5                           | 2.5                                | 0.2   | 3.0                               | 0.2  |
| <b>mean N</b>     | <b>15.0</b>                | <b>5.9</b>                        |                                    |                                    |     |     |                     |                     |                               | <b>2.8</b>                         | <b>1.1</b>  | <b>2.5</b>                        | <b>1.0</b>                                       |
| Reversed polarity |                            |                                   |                                    |                                    |     |     |                     |                     |                               |                                    |   |                                   |  |
| GD15I             | 15.8                       | 1.4                               | 400                                | 570                                | 0.9 | 3.6 | 196.0               | -43.0               | 2.5                           | 2.6                                | 0.2   | 2.6                               | 0.2  |
| GD15B             | 11.7                       | 1.3                               | 540                                | 570                                | 0.7 | 4.4 | 250.7               | -77.5               | 6.9                           | 1.9                                | 0.2   | 1.5                               | 0.2  |
| GD15E             | 2.9                        | 0.3                               | 500                                | 560                                | 0.5 | 4.8 | 227.0               | -64.7               | 5.9                           | 0.5                                | 0.0   | 0.4                               | 0.0  |
| GD27-7            | 7.6                        | 0.4                               | 460                                | 560                                | 0.5 | 9.9 | 198.8               | -72.3               | 1.7                           | 1.2                                | 0.1   | 1.0                               | 0.1  |
| <b>mean R</b>     | <b>9.5</b>                 | <b>5.5</b>                        |                                    |                                    |     |     |                     |                     |                               | <b>1.5</b>                         | <b>0.9</b>  | <b>1.4</b>                        | <b>0.9</b>                                       |

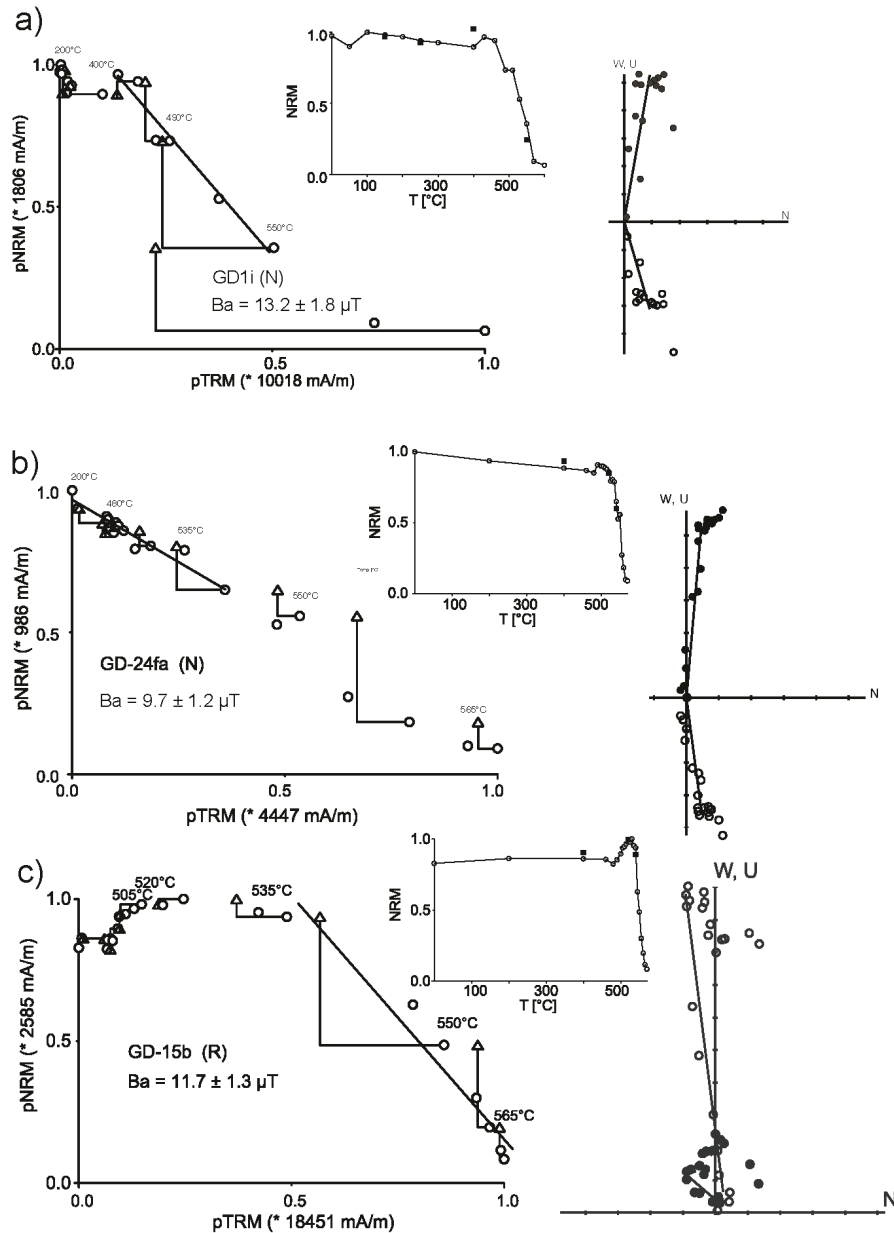


Fig. 9. Examples of paleointensity results from the Central Arizona diabase sheets. The figure represents two N polarities (a,b) and one R polarity case (c). The Arai plot, NRM decay plot with respect to temperature, and the Zijderveld plot are shown from left to right.

## 7. Discussion

The mean directions of the Arizona diabase sheets were based on averaging the 13 normal polarity and 5 reversed polarity sites. It is possible that minor tilting of some diabase sheets have locally taken place, however here we adopted only the correction of *Harlan* (1993) for a consistent rotation of  $5^\circ$  of the Colorado Plateau.

Table 7 shows the site mean directions and corresponding paleopoles of the two polarity groups obtained in this study. The results and the mean directions are also shown in Figure 10a.

Table 7. Grand mean directions from different rock units of the Central Arizona. All data are corrected for 5° rotation. A mean at a reference location for Laurentia (60° N and 275° E) is also displayed. Age data are referred in Table 1.

| Area                          | Rocktype                      | D     | I     | N/n    | k     | $\alpha_{95}$ | Plat | Plong | dp   | A <sub>95</sub> | dm   | References              |
|-------------------------------|-------------------------------|-------|-------|--------|-------|---------------|------|-------|------|-----------------|------|-------------------------|
| <b>Normal Polarity (N1)</b>   |                               |       |       |        |       |               |      |       |      |                 |      |                         |
| Sierra Ancha                  | diabase                       | 283.0 | 52.0  | 6      | -     | -             | 28.0 | 182.0 | -    | -               | -    | Helsley, 1975           |
| Gila County                   | diabase                       | 285.0 | 49.0  | 8      | 56.0  | 9.0           | 27.0 | 179.0 | -    | 6.0             | -    | Helsley et al., 1972    |
| Gila County                   | diabase                       | 278.9 | 45.1  | 17     | 17.9  | 11.0          | 21.3 | 178.0 | 7.0  | 8.8             | 11.0 | Harlan, 1993            |
| Gila County                   | diabase                       | 274.8 | 38.7  | 13/139 | 30.4  | 7.6           | 15.7 | 175.3 | 5.4  | 7.3             | 9.1  | this study              |
| mean                          |                               | 280.3 | 48.2  | 4      | 153.4 | 7.4           | 22.8 | 178.0 | 6.1  | 7.3             | 9.5  |                         |
| at Ref location               |                               | 287.6 | 30.2  | 4      | 153.4 | 7.4           | 22.8 | 178.0 | 6.1  | 7.3             | 9.5  |                         |
| <b>Reversed Polarity (R2)</b> |                               |       |       |        |       |               |      |       |      |                 |      |                         |
| Salt River mc.                | diabase                       | 245.0 | -78.0 | 6      | 28.8  | 12.7          | 41.0 | 278.0 | 22.3 | 23.0            | 23.8 | Sandberg & Butler, 1986 |
| Roosevelt Dam                 | diabase                       | 199.0 | -84.0 | 17     | 47.0  | 5.3           | 45.0 | 254.0 | 10.3 | 10.4            | 10.4 | Elston, p. comm., 1987  |
| Roosevelt Dam                 | baked sed.<br>(Pioneer shale) | 159.0 | -81.0 | 12     | 128.0 | 3.9           | 50.0 | 239.0 | 7.2  | 7.4             | 7.5  | Elston, p. comm., 1987  |
| Gila County                   | diabase                       | 155.2 | -87.5 | 4      | 22.1  | 40.0          | 38.1 | 246.7 | 39.9 | 39.9            | 39.9 | Harlan, 1993            |
| Gila County                   | diabase                       | 193.7 | -78.7 | 5 / 55 | 24.7  | 15.7          | 54.9 | 258.1 | 28.1 | 28.6            | 29.7 | this study              |
| mean                          |                               | 199.1 | -83.1 | 5      | 165.1 | 6.0           | 46.2 | 255.5 | 11.4 | 11.5            | 11.7 |                         |
| at Ref location               |                               | 48.5  | -80.8 | 5      | 165.1 | 6.0           | 46.2 | 255.5 | 11.4 | 11.5            | 11.7 |                         |

The ChRM component in general is thermally isolated between 480 and 580°C, corresponding to magnetite as the primary magnetic phase.

The low paleointensity results and the rejection of various paleomagnetic measurements might as well indicate that remagnetizations are possible.

In particular, site BD shows an R magnetization that can be isolated between 0 and 380°C, or at very high coercivities. This suggests that maghemite would be the carrier of Az R component at this site, and might well be the result of remagnetization. The normal component associated with site BD did not pass our paleomagnetic criteria and so was not used in the final mean. More thermal data from site BD would be needed to get a better idea about these two components.

Unlike previously published, there are also hints about two distinct, symmetric reversal events. The normal polarity site DF is antipodal to the steep upwards reversed component R2, whereas R polarity site SD is antipodal to the moderate shallow normal direction N1 (Fig. 10a). Unfortunately, this symmetry was observed only at these two sites. Anyway, the new observations hint for two symmetric reversals: The first one (R2-N2) has steep upwards/downwards inclination would be followed by a period of rapid APW, from N2 to N1; after that another symmetric reversal with moderate shallow inclinations (N1-R2) occurs.

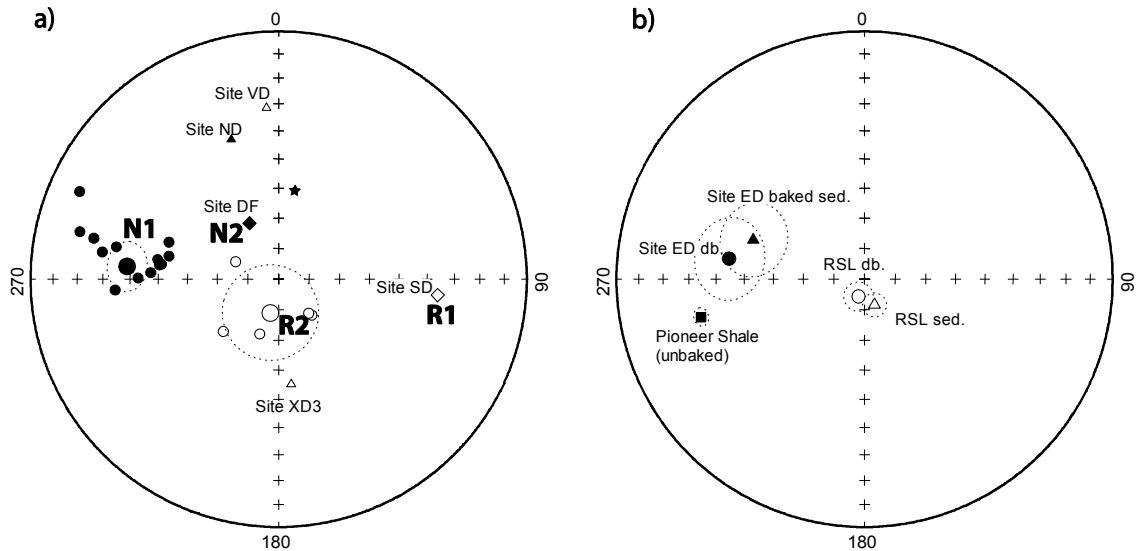


Fig. 10. a) Equal area stereographic projection showing mean directions for each successful site. Circles present accepted sites belonging to the suspected asymmetry. Larger circles are the mean from Table 5. Sites DF and SD, antipodal to the two asymmetric components, are shown as diamonds. Sites VD, ND, and XD3 are rejected based on the rock magnetic and geological analyses. b) Baked contact test performed at site ED with diabases (solid circle) and baked sediments (solid triangle). Additional data after Elston, 1987, pers. comm., show the reversed directions obtained from Roosevelt Dam diabase (open circle) and baked Pioneer Shale (open triangle). The directions are compared with results obtained from the Pioneer Shale (solid square, after *Scott and Paulo*, 1976).

The grand mean direction of the diabase sheets of central Arizona was calculated for both N and R polarities by averaging the available studies (Table 7). The N polarity average is based on the research by *Helsley* (1965), *Helsley and Spall* (1972), *Harlan* (1993), and this study, and yields a mean  $D = 280.3^\circ$ ,  $I = 48.2^\circ$ ,  $\alpha_{95} = 7.4^\circ$ , while the R polarity average is based on the results of *Sandberg and Butler* (1986), *Elston* (1987, pers. comm.), *Harlan* (1993), and this study, and gives a mean  $D = 199.1^\circ$ ,  $I = -83.1^\circ$ ,  $\alpha_{95} = 6.0^\circ$ . The scatter in the obtained directions is comparable with the Model G (*McFadden et al.*, 1988), hence suggesting an average paleosecular variation.

In this study it was possible to perform one baked contact test at site ED (SSR), where the sill yielded reliable results. The baked quartzite (Pioneer Shale, ca. 1.4 Ga; *Fletcher et al.*, 2004) gave a mean direction of  $D = 286.9^\circ$  and  $I = 50.8^\circ$  ( $\alpha_{95} = 11.6^\circ$ ,  $N = 5$ ), which is in agreement with the results obtained from the diabase ( $D = 278.6^\circ$ ,  $I = 44.1^\circ$ ,  $\alpha_{95} = 12.5^\circ$ ,  $N = 6$ , corrected for  $5^\circ$  rotation). The results of the baked contact test from site ED are plotted in an equal area stereoplot (Fig. 10b), together with other results from RSL (*Elston*, 1987, pers. comm.; Table 7) and the Pioneer Shale unbaked direction (*Scott and Paulo*, 1976). Unfortunately, samples located far from the sill ED (unbaked) were not collected. Additional baked sediments were sampled at sites BD (NSR) and JD (RSL), but well defined components could not be determined from sediments at site BD due to complex behavior during demagnetization experiments, and Sill JD did not pass our selection criteria.

Based on the agreement between the magnetization from quartzite samples in the baked contact zone with those of the diabase, we suggest that at least for site ED the

magnetization of the diabase can be considered to be a primary TRM acquired during sill emplacement and cooling. The baked and unbaked directions plot very close to each other, and so a more detailed tectonic study would be necessary to proof that the two are in fact distinct.

Our paleointensity measurements indicate that the field during the sill emplacement (about 1.1 Ga) was low (Fig. 11), consistent with other available studies (Yu *et al.*, 2002; McArdle *et al.*, 2004; Macouin *et al.*, 2006).

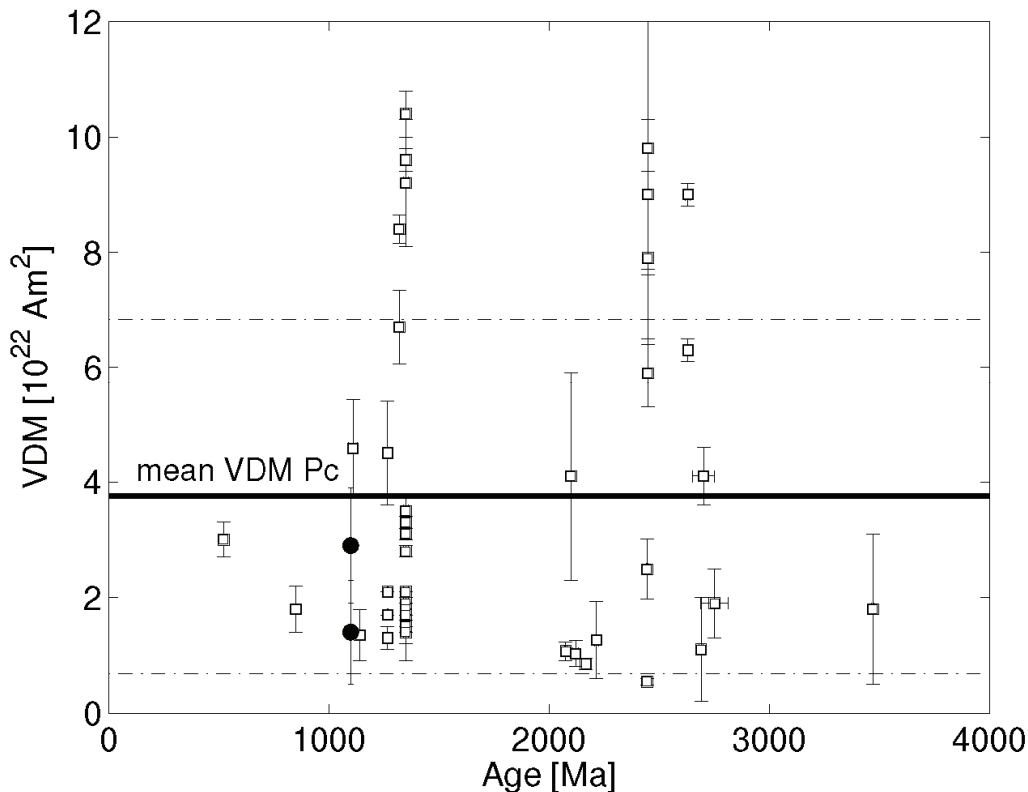


Fig. 11. Mean VDM from the Central Arizona diabase sheets (closed circles), compared with available data for Precambrian (open circles) of the PINT03 database (Perrin and Schnepf, 2004). The mean value from Precambrian data (solid line) and its standard deviation (dashed line) is also shown.

The slow cooling conditions of the diabbases probably favored grain growth and oxyexsolution detectable in the intergrowth of ilmenite-magnetite lamellae. When grains are still growing below the Curie temperature, then the acquired magnetization is a thermochemical remanent magnetization (TCRM). There are various TCRM acquisition scenarios that can lead to overestimates or underestimates of the paleointensity. For example, Smirnov and Tarduno (2005) show that the TCRM efficiency is lower than TRM one, and so the paleointensity would be underestimated up to a factor of 4. Fabian (2009) on the other hand presents cases where, for example, the decrease in volume of the magnetic grains due to leaching can lower the blocking temperature and leads to an increase of the spontaneous magnetization.

The intergrowth of magnetite and ilmenite lamellae observed with the SEM indicate that a certain amount of high temperature oxidation existed. As we do not know

the temperature at which oxyexsolution occurred, we cannot give an absolute value for this bias.

Plotting our paleomagnetic results in terms of Virtual Geomagnetic Poles (VGPs) show consistencies with other available studies (Fig. 12a). Even if lack of absolute ages makes it yet difficult to correlate the various events with each other, the robustness of the loop is corroborated by the stratigraphic series of N polarities from the Grand Canyon studied by *Elston et al.* (2002) shown in Figure 12b. Steep R inclinations were found also at the Grand Canyon, but the publication does not specify to which lithology they belong.

The possibility of two symmetric reversal events acquired at two distinct times remains plausible, but new observations are required to make this a certainty. In this case a very fast drift (from N2 to N1), which we calculated to correspond to about 31cm/a, would be the favoured mechanism to explain the observed loop.

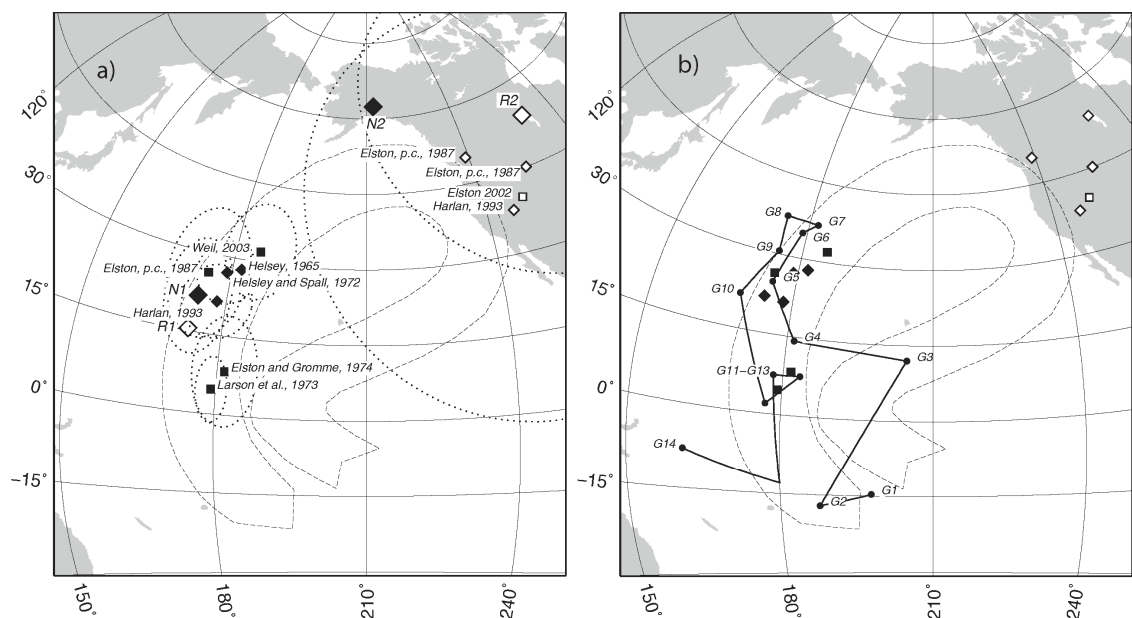


Fig. 12. a) Logan Loop (dashed line), with superimposed poles from the Grand Canyon (diamonds), poles from Central Arizona, and associated  $\alpha_{95}$  (dashed ovals) cones of confidence. b) Labels of the Unkar Loop poles are reported after *Elston et al.* (2002).

## 8. Conclusions

The main results from the 1.1 Ga old Central Arizona diabase study are:

- the rocks show a steep upwards reversed (R) polarity and a moderate shallow downwards normal (N) polarity magnetization.
- Our new data suggest that remagnetization has occurred at some sites (e.g. BD).
- Two sites (DF and SD) suggest that there might be two distinct symmetric reversals (R1-N1 and N2-R2), with considerable plate motion between them (about 30 cm/a). If these observations would be confirmed with measurements

from other independent sites, then the asymmetry would turn out to be an artefact, as recently reported by *Swansson-Hysell et al.* (2009) for the Mamainse point lava flows.

- Thellier paleointensity data reveal a weak field during the emplacement of the diabase sheets. Statistically, the two means for the N and R polarity samples are indistinguishable.

### *Acknowledgments*

This work was funded by the Finnish Academy grant. Discussion with Lisa Tauxe and Jeff Gee provided valuable input for the interpretation of the results. We greatly thank Satu Mertanen and one anonymous reviewer for their thorough comments and suggestions that considerably improved this manuscript.

### *References*

- Banks, N., H. Cornwall, M. Silberman, S. Creasey and R. Marvin, 1972. Chronology of ore intrusion and ore deposition at Ray, Arizona: Part 1, K-Ar ages. *Economic Geology*, **67**, 864–878
- Banks, N., and M. Krieger, 1977. Geologic map of Hayden Quadrangle, Pinal and Gila Counties, Arizona, U.S. Geological Survey Quadrangle Map, GQ1391.
- Borradaile, G.J., K. Lucas, and R.S. Middleton, 2004. Low-temperature demagnetization isolates stable magnetic vector components in magnetite-bearing diabase. *Geophysical Journal International*, **157**, 526–536.
- Coe, R.S., 1967. Paleointensities of the Earth's magnetic field determined from Tertiary and Quaternary rocks. *J. Geophys. Res.*, **72**, 3247–3262.
- D'AgrellaFilho, M.S., I.G. Pacca, P.R. Renne, T.C. Onstott, and W. Teixeira, 1990. Paleomagnetism of middle Proterozoic, (1.01 to 1.08 Ga) mafic dykes in southeastern Bahia State – Sao Francisco Craton, Brazil. *Earth and Planetary Science Letters*, **101**, 332–348.
- D'AgrellaFilho, M.S., I.G. Pacca, R.I.F. Trindade, W. Teixeira, M. Irene, B. Raposo, and T.C. Onstott, 2004. Paleomagnetism and ArAr ages of mafic dykes from Salvador, Brazil): new constraints on the Sao Francisco Craton APW path between 1080 and 1010 Ma. *Precambrian Research*, **132**, 55–77.
- Damon, P.E., D.E. Livingstone and R.C. Erickson, 1962. New K-Ar dates for the Precambrian of Pinal, Gila, Yavapai and Coconino countries, Arizona. In: 13<sup>th</sup> Field Conference Guidebook, 56–57, New Mexico Geological Society
- Day, R., M.D. Fuller, and V.A. Schmidt, 1977. Hysteresis properties of titanomagnetites: grain size and composition dependence. *Physics of the Earth and Planetary Interiors*, **13**, 260–266.
- Dunlop, D., 2002. Theory and application of the Day plot, Mrs/Ms versus Hcr/Hc) 1. Theoretical curves and tests using titanomagnetite data. *J. Geophys. Res.*, **107**, doi:10.1029/2001JB000486.

- Elston, D.P., R.J. Enkin, J. Baker, and D.K. Kisilevsky, 2002. Tightening the Belt: Paleomagnetic-stratigraphic constraints on deposition, correlation, and deformation of the Middle Proterozoic, ca. 1.4 Ga, Belt Purcell Supergroup, United States and Canada. *Geological Society of America Bulletin*, **114**, 619–638.
- Ernst, R.E., and K.L. Buchan, 1993. Paleomagnetism of the Abitibi dyke swarm, southern Superior Province, and implications for the Logan Loop. *Canadian Journal of Earth Sciences*, **30**, 1886–1897.
- Ernst, R.E., and K.L. Buchan, 2003. Recognizing mantle plumes in the geological record. *Annual Reviews Earth Planetary Sciences*, **31**, 469–523.
- Evans, D., 2003. True polar wander and supercontinents. *Tectonophysics*, **362**, 303–320.
- Fletcher, K.E., M.T. Heizler, K. Karlstrom, J.M. Timmons, L.J. Crossey and J.D. Bloch, 2004. Provenance and geochronology of Mesoproterozoic sedimentary rocks from across the Southwest United States revealed by  $^{40}\text{Ar}$ - $^{39}\text{Ar}$  dating of detrital muscovites, in GSA Annual Meeting and Exposition, Abstracts with Programs, **36**, 405, Geological Society of America.
- Gallet, Y. and M. LeGoff, 2006. Hightemperature archeointensity measurements from Mesopotamia. *Earth and Planetary Science Letters*, **241**, 159–173.
- Gose, W.A., M.A. Helper, J.N. Connelly, F.E. Hutson and I.W.D. Dalziel, 1997. Paleomagnetic data and U-Pb isotopic age determinations from Coats Land, Antarctica: implications for Late Proterozoic plate reconstructions. *J. Geophys. Res.*, **102**, 7887–7902.
- Hammond, J.G., 1986. Geochemistry and petrogenesis of Proterozoic diabase in the southern Death Valley region of California. *Contributions to Mineralogy and Petrology*, **93**, 312–321.
- Hammond, J.G. and J.L. Wooden, 1986. Isotopic constraints on the petrogenesis of Proterozoic diabase in southwestern USA. In: A. Parker, P. Rickwood and D. Rucker, (eds.), Mafic dykes and emplacement mechanism, 145–156, Balkeema, Rotterdam.
- Hanson, R.E., J.L. Crowley, S.A. Bowring, J. Ramezani, W.A. Gose, I.W.D. Dalziel, J.A. Pancake, E.K. Seidel, T.G. Blenkinsop and J. Mukwakwami, 2004. Coeval largescale magmatism in the Kalahari and Laurentian cratons during Rodinia assembly. *Science*, **304**, 1126–1129.
- Harlan, S., 1992. Paleomagnetism and  $^{40}\text{Ar}$ - $^{39}\text{Ar}$  eochronology of selected Proterozoic intrusions, southwest Montana, southeastern Wyoming, and central Arizona., 192 pp., Ph.D. Thesis, University of New Mexico.
- Harlan, S., 1993. Paleomagnetism of Middle Proterozoic diabase sheets from central Arizona. *Canadian Journal of Earth Sciences*, **30**, 1415–1426.
- Heaman, L.M. and J.P. Grotzinger, 1992. 1.08 Ga diabase sill in the Pahrump Group, California; implications for the development of the Cordilleran miogeocline. *Geology*, **20**, 637-640

- Helsley, C.E., 1965. Paleomagnetic results from Precambrian rocks of Central Arizona and Duluth, Minnesota. *EOS Transactions of the American Geophysical Union*, **67**, 46.
- Helsley, C.E. and H. Spall, 1972. Paleomagnetism of 1140 to 1150 Million year diabase sills from Gila County, Arizona. *J. Geophys. Res.*, **77**, 2115–2128.
- Hendricks, J.D., 1972. Younger Precambrian basaltic rocks from the Grand Canyon, Arizona. MSc. Thesis, Northern Arizona University.
- Hnat, J., B. Van der Pluijm and R. Van der Voo, 2006. Primary curvature in the MidContinent Rift: Paleomagnetism of the Portage Lake Volcanics, northern Michigan, USA. *Tectonophysics*, **425**, 71–82, doi:0.1016/j.tecto.2006.07.006.
- Howard, K., 1991. Intrusion of horizontal dykes: tectonic significance of Middle Proterozoic diabase sheets in the upper crust of Southwestern United States, *J. Geophys. Res.*, **96**, 12,461–12,478.
- Kumar, A., L. Heaman and C. Manikyamba, 2007. Mesoproterozoic kimberlites in South India A possible link to ca. 1.1 Ga global magmatism. *Precambrian Research*, **154**, 192–204.
- Leonhardt, R., C. Heunemann and D. Krasa, 2004. Analyzing absolute palaeointensity determination: acceptance criteria and the software Thellier tool. *Geochemistry, Geophysics, Geosystems*, **5**. doi:10.1029/2004GC000,807.
- Macouin, M., J.P. Valet, J. Besse and R. Ernst, 2006. Absolute paleointensity at 1.27 Ga from the Mackenzie dyke swarm, Canada. *Geophysics, Geochemistry, and Geosystems*, **7**, Q01H21, doi:10.1029/2005GC000,960.
- McArdle, N.J., H. Halls and J. Shaw, 2004. Microwave palaeointensities from 1.1Ga Keweenawan dykes, Ontario. *Geophysical Research Abstracts*, vol. **6**, 06433, European Geosciences Union.
- McFadden, P.L., R.T. Merrill and M.W. McElhinny, 1988. Dipole/Quadrupole Family Modeling of Paleosecular Variation. *J. Geophys. Res.*, **93**(B10), 583–588
- McKey, E.H. and D.C. Noble, 1976. Age of the Cardenas lavas, Grand Canyon, Arizona. *Geological Society of America Bulletin*, **81**, 1733–1766
- Mertanen, S., L.J. Pesonen and H. Huhma, 1996. Palaeomagnetism and Sm-Nd ages of the Neoproterozoic diabase dykes in Laanila and Kautokeino, northern Fennoscandia. *Geological Society, London, Special Publications*, **112**, 331-358
- Nehru, C.E. and M. Prinz, 1970. Petrologic study of the Sierra Ancha sill complex, Arizona. *Geological Society of America Bulletin*, **81**, 1733–1766.
- Palmer, H., 1970. Paleomagnetism and correlation of some Middle Keweenawan rocks, Lake Superior. *Canadian Journal of Earth Sciences*, **7**, 1410–1436.
- Perrin, M. and E. Schnepp, 2004. IAGA paleointensity database: Distribution and quality of the data set. *Physics of the Earth and Planetary Interiors*, **147**, 255–267.
- Pesonen, L. and H. Halls, 1983. Geomagnetic field intensity and reversal asymmetry in late Precambrian Keweenawan rocks. *Geophysical Journal of the Royal Astronomical Society*, **73**, 241–270.

- Pesonen, L. and H. Nevanlinna, 1981. Late Precambrian Keeweenawan asymmetric reversal. *Nature*, **294**, 436–439.
- Powell, C.A., D.L. Jones, S. Pisarevsky and M.T.D. Wingate, 2001. Palaeomagnetic constraints on the position of the Kalahari craton in Rodinia. *Precambrian Research*, **110**, 33–46.
- Riisager, P. and J. Riisager, 2001. Detecting multidomain magnetic grains in Thellier paleointensity experiments. *Physics of the Earth and Planetary Interiors*, **125**, 111–117.
- Salminen, J., L.J. Pesonen, S. Mertanen, J. Vuollo and M.-L. Airo, 2009. Palaeomagnetism of the Salla Diabase Dyke, northeastern Finland, and its implication for the Baltica-Laurentia entity during the Mesoproterozoic. *Geological Society, London, Special Publications*, **323**, 199–217.
- Sandberg, S.A. and R.F. Butler, 1986. Paleomagnetic fold test evidence of monoclinical folding, Salt River Canyon, Arizona. *Earth and Planetary Science Letters*, **73**, 140–146.
- Scott G.R. and C.P. Paulo, 1976. Paleomagnetism of the Pioneer Shale (1300–1350 M.y.) and associated high temperature TRM. *EOS, Transactions of the American Geophysical Union*, **57**, 902
- Shastri, L., K. Chamberlin and S. Bowring, 1991. Inherited zircon from ca. 1.1 Ga mafic dikes, NW Arizona. *Geological Society of America, Abstract with Programs*, **23**, 93
- Shride, A.F., 1967. Younger Precambrian geology in southern Arizona. *U.S. Geological Survey Professional Paper*, **566**, 89 pp.
- Silver, L.T., 1960. Age determination of Precambrian diabase differentiates in the Sierra Ancha, Gila County, Arizona. *Geological Society of American Bulletin*, **71**, 1973–1974.
- Silver, L.T., 1963. The use of current Uranium/Lead isotope systems in geochronology. *Geological Society of American Bulletin*, **74**, 279–285.
- Silver, L.T., 1978. Precambrian formation in Precambrian history. In: Land of Cochise, 157–163. New Mexico Geological Society guidebook.
- Smirnov, A. and J. Tarduno, 2005. Thermochemical remanent magnetization in pre-cambrian rocks: Are we sure the geomagnetic field was weak? *Journal of Geophysical Research*, **110**, Art. No. B06,103.
- Smith, D., 1970. Mineralogy of the diabase rocks in a differentiated olivine diabase sill complex, Sierra Ancha, Arizona. *Contributions to Mineralogy and Petrology*, **27**, 95–113.
- Spencer, J., C. Isachsen, C. Ferguson, S. Richard, S. Skotnicki, J. Wooden and N. Riggs, 2003. U-Pb isotope geochronologic data from 23 igneous rock units in central and Southeastern Arizona, 40 pp. Arizona Geological Survey, Open file report 03–08, Arizona.
- Steiner, M., 2003. A cratonic Middle Jurassic paleopole: Callovian Oxfordian stillstand, J2 cusp. rotation of the Colorado Plateau, and Jurassic North American apparent polar wander. *Tectonics*, **22**, doi:10.1029/2001TC001,284.

- Swanson-Hysell, N.L., A.C. Maloof, D.A.D. Evans and B.P. Weiss, 2009. No asymmetry in geomagnetic reversals recorded by 1.1-billion-year-old Keweenawan basalts. *Nature Geoscience*, **2**, 713-717.
- Tarduno, J.A. and A.V. Smirnov, 2004. The paradox of low field values and the long term history of the geodynamo, in Timescales of the paleomagnetic field, edited by J. Channell, D. Kent, W. Lowrie and J. Meert, pp. 75–84, *American Geophysical Union, Geophysical Monographs* **145**.
- Tauxe, L., with the contributions from R. Butler, R. van der Voo and S. Banerjee, 2010. *Essentials of Paleomagnetism*, University of California Press, 489 pp.
- Timmons, J.M., K.E. Karlstrom, M.T. Heizler, S.A. Bowring, G.E. Gehrels and L. Crossey, 2005. Tectonic inference from the ca. 1255–1100 Ma Unkar Group and Nankoweap Formation, Grand Canyon: Intracratonic deformation and basin formation during protracted Grenville orogenesis, *Geological Society of America Bulletin*, **117**, 1573–1595.
- Weil, A.B., J.W. Geissman, M. Heizler and R. Van der Voo, 2003. Paleomagnetism of the Middle Proterozoic mafic intrusions and Upper Proterozoic, Nankoweap) red beds from the Lower Grand Canyon Supergroup, Arizona. *Tectonophysics*, **375**, 199–220.
- Wessel, P. and W. Smith, 1991. Free software helps map and display data. *Eos Trans. AGU*, **72**, 441.
- Wrucke, C.T., 1989. The Middle Proterozoic Apache group, Troy quartzite, and associated diabase of Arizona, in Geologic evolution of Arizona, vol. 17, edited by J. Jenny and S. Reynolds, pp. 239–258, Arizona Geological Society Digest.
- Yu, Y., D. Dunlop, L. Pavlish, and M. Cooper, 2002. Multivectorial paleointensity determination from the Cordova Gabbro, southern Ontario. *Earth and Planetary Science Letters*, **203**, 983–998.